hep-ph/9906481
OHSTPY-HEP-T-99-013
KEK-TH-632

Stability of the Lepton-Flavor Mixing Matrix Against Quantum Corrections

N. Haba[1,2*] and N. Okamura[3†]

[1] *Department of Physics, The Ohio State University, Columbus, Ohio 43210, USA*

[2] *Faculty of Engineering, Mie University, Tsu Mie 514-8507, Japan*

[3] *Theory Group, KEK, Tsukuba Ibaraki 305-0801, Japan*

Abstract

Recent neutrino experiments suggest the strong evidences of tiny neutrino masses and the lepton-flavor mixing. Neutrino-oscillation solutions for the atmospheric neutrino anomaly and the solar neutrino deficit can determine the texture of neutrino mass matrix according to the neutrino mass hierarchies as Type A: $m_3 \gg m_2 \sim m_1$, Type B: $m_3 \ll m_2 \sim m_1$, and Type C: $m_3 \sim m_2 \sim m_1$. In this paper we study the stability of the lepton-flavor mixing matrix against quantum corrections for all types of mass hierarchy in the minimal supersymmetric Standard Model with the effective dimension-five operator which gives Majorana masses of neutrinos. The relative sign assignments of neutrino masses in each type play the crucial roles for the stability against quantum corrections. We find the lepton-flavor mixing matrix of Type A is stable against quantum corrections, and that of Type B with the same (opposite) signs of m_1 and m_2 are unstable (stable). For Type C, the lepton-flavor-mixing matrix approaches to the definite unitary matrix according to the relative sign assignments of neutrino mass eigenvalues, as the effects of quantum corrections become large enough to neglect squared mass differences of neutrinos.

PACS NUMBER:
12.15.Ff, 14.60.Pq, 23.40.Bw
KEY WORDS:
Lepton Flavor Mixing, Renormalization Effect

*E-mail address:haba@pacific.mps.ohio-state.edu
†E-mail address:naotoshi.okamura@kek.jp

1 Introduction

Recent neutrino experiments suggest the strong evidences of tiny neutrino masses and the flavor mixing in the lepton sector [1]-[4]. Studies of the lepton-flavor-mixing matrix, which is called Maki-Nakagawa-Sakata (MNS) matrix [5], point to new steps of the flavor physics. Especially, study of the energy-scale dependence of the MNS matrix is one of the main issues to investigate the new physics beyond the Standard Model (SM) [6].

There are following neutrino-oscillation solutions for the solar neutrino deficit and the atmospheric neutrino anomaly:

$$\Delta m^2_{\rm solar} = \begin{cases} 0.85\times 10^{-10} & {\rm eV}^2 \quad \text{(vacuum solution)}, \\ 1.8\times 10^{-5} & {\rm eV}^2 \quad \text{(MSW-large mixing solution)}, \\ 0.8\times 10^{-5} & {\rm eV}^2 \quad \text{(MSW-small mixing solution)}, \end{cases} \tag{1.1a}$$

$$\Delta m^2_{\rm ATM} = 3.7\times 10^{-3} \ \ {\rm eV}^2\,, \tag{1.1b}$$

where $\Delta m^2_{\rm solar}$ and $\Delta m^2_{\rm ATM}$ stand for the squared mass differences of the solar neutrino deficit [1] and the atmospheric neutrino anomaly [2, 3], respectively. In this article, we adopt the scenario of three generation neutrinos which means

$$\Delta m^2_{\rm solar} \equiv \left| m_2^2 - m_1^2 \right| , \quad \text{and} \quad \Delta m^2_{\rm ATM} \equiv \left| m_3^2 - m_2^2 \right| , \tag{1.2}$$

where m_i is the i-th ($i = 1 \sim 3$) generation neutrino mass ($m_i \geq 0$). We take the following values of the mixing angles for their solutions.

$$\sin^2 2\theta_{\rm solar} = \begin{cases} 1 & \text{(vacuum solution)}, \\ 1 & \text{(MSW-large mixing solution)}, \\ 0.017 & \text{(MSW-small mixing solution)}, \end{cases} \tag{1.3a}$$

$$\sin^2 2\theta_{\rm ATM} = 1 \qquad \text{(atmospheric neutrino anomaly)}\,, \tag{1.3b}$$

$$\sin^2 2\theta_{\rm CHOOZ} = 0 \qquad \text{(CHOOZ experiment)}\,. \tag{1.3c}$$

Under the assignments of eqs.(1.2), there are three possible types of neutrino mass hierarchy [7] as

$$\text{Type A} \ : \ m_3 \gg m_2 \sim m_1\,, \tag{1.4a}$$

$$\text{Type B} \ : \ m_1 \sim m_2 \gg m_3\,, \tag{1.4b}$$

$$\text{Type C} \ : \ m_3 \sim m_2 \sim m_1\,. \tag{1.4c}$$

In this article, we study the stability of the MNS matrix for these three types of neutrino mass hierarchy against quantum corrections in the minimal supersymmetric Standard

Model (MSSM) with the effective dimension-five operator which gives Majorana masses of neutrinos. Since the negative sign assignments of m_i in eqs.(1.4) also satisfy eqs.(1.2), we consider all relative sign assignments for masses in each type. We determine the MNS matrix elements at the low energy scale from results of neutrino-oscillation experiments, and analyze whether the MNS matrix is stable against quantum corrections or not in each type of neutrino mass hierarchy. The results of analyses strongly depend on the types of neutrino mass hierarchy and the relative sign assignments of masses as follows.

Type A: The MNS matrix is stable against quantum corrections.
Type B: The MNS matrix is unstable (stable) when m_1 and m_2 have the same (opposite) signs.
Type C: The MNS matrix approaches to the definite unitary matrix according to the relative sign assignments of neutrino masses, as the effects of quantum corrections become large enough to neglect squared masse differences of neutrino.

We also study the stability of the MNS matrix against quantum corrections in the two generation neutrinos. Results of this article are not only useful for the model building beyond the SM, but also show the possibility to obtain the large mixing angles from quantum corrections.

This article is organized as follows. In section 2, we determine the elements of the MNS matrix from the data of recent neutrino-oscillation experiments. In section 3, we estimate the magnitude of quantum corrections of the dimension-five Majorana operator. In section 4, we study the stability of the MNS matrix against renormalization effects in the two generation neutrinos. In section 5, we analyze the stability of the MNS matrix against quantum corrections in the three generation neutrinos for each type of mass hierarchy. Section 6 gives the conclusion.

2 The Maki-Nakagawa-Sakata Matrix

In this section, we give the definition and the parameterization of the Maki-Nakagawa-Sakata (MNS) lepton-flavor mixing matrix [5]. We determine elements of the MNS matrix from the data of recent neutrino-oscillation experiments [1]-[4].

2.1 Definition

The effective Yukawa Lagrangian in the lepton sector is given by

$$\mathcal{L}^{\rm low}_{yukawa} = y^{\rm e}{}_{ij}\phi_{\rm d}L_i\cdot e^c_{Rj} - \frac{1}{2}\kappa_{ij}(\phi_{\rm u}L_i)\cdot(\phi_{\rm u}L_j) + h.c.\,, \tag{2.1}$$

where $y^{\rm e}_{ij}$ is the Yukawa matrix of the charged lepton. $\phi_{\rm u}$ and $\phi_{\rm d}$ are the SU(2)$_L$ doublet Higgs bosons that give Dirac masses to the up-type and the down-type fermions, respectively. L_i is the i-th generation SU(2)$_L$ doublet lepton. e_{Ri} is the i-th generation charged lepton. κ induces the neutrino Majorana mass matrix which is complex and symmetric.

Now we give the definition of the 3×3 MNS matrix, which is defined on the analogy of the CKM matrix [8, 9]. Unitary matrices of $U_{\rm e}$ and U_ν transform the mass-eigenstates into the weak-current eigenstates as

$$\begin{pmatrix} l_{L1} \\ l_{L2} \\ l_{L2} \end{pmatrix} = U_{\rm e} \begin{pmatrix} e_L \\ \mu_L \\ \tau_L \end{pmatrix}, \qquad \begin{pmatrix} \nu_{L1} \\ \nu_{L2} \\ \nu_{L3} \end{pmatrix} = U_\nu \begin{pmatrix} \nu_1 \\ \nu_2 \\ \nu_3 \end{pmatrix}. \tag{2.2}$$

The MNS matrix is then defined as

$$(V_{\rm MNS})_{\alpha i} \equiv \left(U_{\rm e}^\dagger U_\nu\right)_{\alpha i}, \qquad \nu_\alpha = \sum_{i=1}^{3} (V_{\rm MNS})_{\alpha i}\, \nu_i\,, \tag{2.3}$$

where α and i label the neutrino flavors ($\alpha = e, \mu, \tau$) and the mass eigenstates ($i = 1, 2, 3$), respectively.

2.2 Parameterization

The 3×3 MNS matrix has three mixing angles and three physical phases in general for the Majorana neutrinos. We adopt the parameterization of

$$V_{\rm MNS} = \underbrace{\begin{pmatrix} U_{e1} & U_{e2} & U_{e3} \\ U_{\mu 1} & U_{\mu 2} & U_{\mu 3} \\ U_{\tau 1} & U_{\tau 2} & U_{\tau 3} \end{pmatrix}}_{U_{\alpha i}} \begin{pmatrix} 1 & 0 & 0 \\ 0 & e^{i\varphi_2} & 0 \\ 0 & 0 & e^{i\varphi_3} \end{pmatrix}. \tag{2.4}$$

The matrix $U_{\alpha i}$, which has three mixing angles and one phase, can be parameterized as the same way as the CKM matrix. Since the data of the present neutrino-oscillation experiments directly constrain elements of U_{e2}, U_{e3}, and $U_{\mu 3}$, the most convenient parameterization is to adopt these three elements as the independent parameters [10, 11, 12]. Without losing generality, we can take U_{e2} and $U_{\mu 3}$ to be real and non-negative by the redefinition of φ_2 and φ_3. Then only U_{e3} has a complex phase. All the other matrix elements can be determined by the unitarity conditions as follows.

$$
\begin{aligned}
U_{e1} &= \sqrt{1-|U_{e3}|^2-|U_{e2}|^2}\,, & U_{\tau 3} &= \sqrt{1-|U_{e3}|^2-|U_{\mu 3}|^2}\,, \\
U_{\mu 1} &= -\frac{U_{e2}U_{\tau 3}+U_{\mu 3}U_{e1}U_{e3}^*}{1-|U_{e3}|^2}\,, & U_{\mu 2} &= \frac{U_{e1}U_{\tau 3}-U_{\mu 3}U_{e2}U_{e3}^*}{1-|U_{e3}|^2}\,, \\
U_{\tau 1} &= \frac{U_{e2}U_{\mu 3}-U_{\tau 3}U_{e1}U_{e3}^*}{1-|U_{e3}|^2}\,, & U_{\tau 2} &= -\frac{U_{\mu 3}U_{e1}+U_{e2}U_{\tau 3}U_{e3}^*}{1-|U_{e3}|^2}\,.
\end{aligned}
\tag{2.5}
$$

Here U_{e1}, U_{e2}, $U_{\mu 3}$, and $U_{\tau 3}$ are real and non-negative, and the other elements are complex.

The relations among the MNS matrix elements and the mixing angles are given by

$$
\sin\theta_{13} = |U_{e3}|\,, \quad \sin\theta_{23} = \frac{U_{\mu 3}}{\sqrt{1-|U_{e3}|^2}}\,, \quad \sin\theta_{12} = \frac{U_{e2}}{\sqrt{1-|U_{e3}|^2}}\,, \tag{2.6}
$$

which can be rewritten by

$$
\sin^2 2\theta_{13} = 4|U_{e3}|^2\left(1-|U_{e3}|^2\right)\,, \tag{2.7a}
$$

$$
\sin^2 2\theta_{23} = 4\frac{U_{\mu 3}^2}{1-|U_{e3}|^2}\left(1-\frac{U_{\mu 3}^2}{1-|U_{e3}|^2}\right)\,, \tag{2.7b}
$$

$$
\sin^2 2\theta_{12} = 4\frac{U_{e2}^2}{1-|U_{e3}|^2}\left(1-\frac{U_{e2}^2}{1-|U_{e3}|^2}\right)\,, \tag{2.7c}
$$

where θ_{ij} is the mixing angle between the i-th and j-th generations. In general, these mixing angles are not the same as those obtained from the two generation analyses of the experimental results.

2.3 The MNS matrix at the weak scale

Now let us decide the values of U_{e2}, U_{e3} and $U_{\mu 3}$, which are independent parameters of the MNS matrix, from the data of neutrino-oscillation experiments* .

2.3.1 U_{e3}

The CHOOZ experiment [4] measures the survival probability of $\overline{\nu_e}$. The result of this experiment shows

$$
\sin^2 2\theta_{\rm CHOOZ} < 0.18\,, \quad \text{for} \quad \delta m^2_{\rm CHOOZ} > 1\times 10^{-3}{\rm eV}^2. \tag{2.8}
$$

*Neutrino-oscillation probabilities are shown in Appendix A.

From eq.(A.5), we can obtain the following constraint

$$|U_{e3}|^2 \left(1 - |U_{e3}|^2\right) < 0.045\,, \tag{2.9a}$$

$$\text{for} \quad |m_3^2 - m_1^2| \simeq |m_3^2 - m_2^2| > 1 \times 10^{-3}\text{eV}^2\,. \tag{2.9b}$$

In this article we assume the (1,3) element of the MNS matrix at the weak scale m_z to be

$$U_{e3} = 0\,. \tag{2.10}$$

2.3.2 $U_{\mu 3}$

The atmospheric neutrino data [2, 3] suggest the maximal mixing of $\nu_\mu \to \nu_X$ ($\nu_X \neq \nu_\mu, \nu_e$) oscillation[†]. In the three-flavor analysis, the most reliable interpretation of the data is $\nu_\mu \to \nu_\tau$ oscillation under the condition of eq.(A.3). From eqs.(2.7b), (2.10) and (A.5), we can obtain

$$\sin^2 2\theta_{\text{ATM}} = 4U_{\mu 3}^2 \left(1 - U_{\mu 3}^2\right)\,. \tag{2.11}$$

Thus, by using eq.(1.3b) we determine the (2,3) element of the MNS matrix at the m_z scale as

$$U_{\mu 3} = \frac{1}{\sqrt{2}}\,. \tag{2.12}$$

2.3.3 U_{e2}

Deficits of solar neutrinos observed at several telestial experiments [1] have been interpreted as $\nu_e \to \nu_X$ ($\nu_X \neq \nu_e\,, \overline{\nu_e}$) oscillation of the three solutions, which are the MSW small-mixing solution (MSW-S), the MSW large-mixing solution (MSW-L) [13], and the vacuum oscillation solution (VO) [14]. By using eq.(2.10), the survival probability of ν_e in eq.(A.8) is simplified as

$$P_{\nu_e \to \nu_e} = 1 - 4|U_{e1}|^2 |U_{e2}|^2 \sin^2 \left(\frac{\delta m_{12}^2}{4E} L\right)\,. \tag{2.13}$$

Equation (2.10) also simplifies eq.(2.7c) to be

$$\sin^2 2\theta_{\text{SUN}} = 4U_{e2}^2 \left(1 - U_{e2}^2\right)\,. \tag{2.14}$$

Thus, from eqs.(1.3a), we determine the value of U_{e2} at the m_z scale as

$$\text{MSW-S} : U_{e2} = 0.0042\,, \quad \text{MSW-L} : U_{e2} = \frac{1}{\sqrt{2}}\,, \quad \text{VO} : U_{e2} = \frac{1}{\sqrt{2}}\,, \tag{2.15}$$

for each solution.

[†]The oscillation of $\nu_\mu \to \nu_e$ is not only disfavored by the CHOOZ experiment data of eq.(2.8), but also disfavored by the Super-Kamiokande data by itself [2, 3].

2.3.4 The MNS matrix at m_z scale

In this article we neglect Majorana phases of $\varphi_{2,3}$ in the MNS matrix of eq.(2.4) for simplicity. By using eqs.(2.5), (2.10) and (2.12), the MNS matrix at the m_z scale is determined as

$$U_{\rm MNS} = \begin{pmatrix} \cos\theta & \sin\theta & 0 \\ \dfrac{-\sin\theta}{\sqrt{2}} & \dfrac{\cos\theta}{\sqrt{2}} & \dfrac{1}{\sqrt{2}} \\ \dfrac{\sin\theta}{\sqrt{2}} & \dfrac{-\cos\theta}{\sqrt{2}} & \dfrac{1}{\sqrt{2}} \end{pmatrix}, \tag{2.16}$$

where $\theta^{\ddagger}$ depends on the solution of the solar neutrino deficits as

$$\sin\theta = \begin{cases} 0.0042 & (\theta = 0.0042) & ({\rm MSW\text{-}S}), \\ \dfrac{1}{\sqrt{2}} & (\theta = \dfrac{\pi}{4}) & ({\rm MSW\text{-}L}), \\ \dfrac{1}{\sqrt{2}} & (\theta = \dfrac{\pi}{4}) & ({\rm VO}), \end{cases} \tag{2.17}$$

which are obtained from eqs.(2.15).

3 Quantum Corrections of κ

The renormalization group equation (RGE) of κ, which is the coefficient of dimension-five operator in the effective Lagrangian of eq.(2.1), has been studied in Refs. [15, 16]. It is expected that κ is produced by the see-saw mechanism [17] at the high energy-scale M_R. In the MSSM, κ satisfies the following RGE at the one-loop level [16]:

$$8\pi^2 \frac{d}{dt}\kappa = \left\{ {\rm tr}\left(3y^{\rm u}y^{\rm u\dagger}\right) - 4\pi\left(3\alpha_2 + \frac{3}{5}\alpha_1\right)\right\}\kappa + \frac{1}{2}\left\{\left(y^{\rm e}y^{\rm e\dagger}\right)\kappa + \kappa\left(y^{\rm e}y^{\rm e\dagger}\right)^T\right\}, \tag{3.1}$$

where $t = \ln\mu$, and μ is the renormalization scale. $y^{\rm u}$ is the up-quark Yukawa matrix. We notice that once $y^{\rm e}$ is taken diagonal, this form is kept thought all energy-scale at the one-loop level. It is because there are no lepton-flavor-mixing terms except for κ in the MSSM Lagrangian. In this base κ is diagonalized by the MNS matrix, and eq.(3.1) is simplified to be

$$8\pi^2 \frac{d}{dt}\ln\kappa_{ij} = {\rm tr}\left(3y^{\rm u}y^{\rm u\dagger}\right) - 4\pi\left(3\alpha_2 + \frac{3}{5}\alpha_1\right) + \frac{1}{2}\left(y_i^2 + y_j^2\right), \tag{3.2}$$

‡From now on, θ_{12} is denoted by θ unless we note explicitly.

where y_i $(i = 1 \sim 3)$ stands for the i-th generation charged-lepton Yukawa coupling.

The RGE of κ has two important features[§]. One is that none of the phases in κ depend on the energy-scale. The other is that the RGE of κ can be governed by only n_g equations, where n_g stands for the generation number. In the three generation case ($n_g = 3$), κ can be parameterized as

$$\begin{aligned}\kappa &= \kappa_{33} \begin{pmatrix} r_1 & c_{12}\sqrt{r_1 r_2} & c_{13}\sqrt{r_1} \\ c_{12}\sqrt{r_1 r_2} & r_2 & c_{23}\sqrt{r_2} \\ c_{13}\sqrt{r_1} & c_{23}\sqrt{r_2} & 1 \end{pmatrix}, \\ &= \kappa_{33} \begin{pmatrix} \sqrt{r_1} & 0 & 0 \\ 0 & \sqrt{r_2} & 0 \\ 0 & 0 & 1 \end{pmatrix} \begin{pmatrix} 1 & c_{12} & c_{13} \\ c_{12} & 1 & c_{23} \\ c_{13} & c_{23} & 1 \end{pmatrix} \begin{pmatrix} \sqrt{r_1} & 0 & 0 \\ 0 & \sqrt{r_2} & 0 \\ 0 & 0 & 1 \end{pmatrix}. \end{aligned} \tag{3.3}$$

Here c_{ij}s $(i = 1, 2$ and $j = 2, 3)$ are defined as

$$c_{ij}^2 \equiv \frac{\kappa_{ij}^2}{\kappa_{ii}\kappa_{jj}}, \tag{3.4}$$

which are energy-scale independent complex parameters. r_is in eq.(3.3) are defined as

$$r_i \equiv \frac{\kappa_{ii}}{\kappa_{33}}, \qquad (i = 1, 2), \tag{3.5}$$

which are always taken real and non-negative by the redefinitions of lepton fields. Since the MNS matrix is independent of the overall factor κ_{33}, only two real parameters, r_1 and r_2, determine the energy-scale dependence of the MNS matrix.

From eq.(3.2), the RGE of r_i is given by

$$\frac{d}{dt}\ln r_i = \frac{d}{dt}\ln\frac{\kappa_{ii}}{\kappa_{33}} = -\frac{1}{8\pi^2}\left(y_\tau^2 - y_i^2\right), \quad (i = 1, 2), \tag{3.6}$$

where y_τ is Yukawa coupling of τ. Since the right-hand side of eq.(3.6) is always negative, the value of r_i decreases as the energy-scale increases. Equation (3.6) can be solved as

$$r_i(M_R) = r_i(m_z)\frac{I_i}{I_\tau}, \tag{3.7}$$

where I_i $(i = 1(e), 2(\mu), \tau)$ is defined as

$$I_i \equiv \exp\left(\frac{1}{8\pi^2}\int_{\ln(m_z)}^{\ln(M_R)} y_i^2\, dt\right). \tag{3.8}$$

[§] More detail discussions are in the Ref. [18].

From eqs.(3.3) and (3.7), κ at the M_R scale is determined as

$$\kappa(M_R) = \frac{\kappa_{33}(M_R)}{\kappa_{33}(m_z)} \begin{pmatrix} \sqrt{I_e/I_\tau} & 0 & 0 \\ 0 & \sqrt{I_\mu/I_\tau} & 0 \\ 0 & 0 & 1 \end{pmatrix} \kappa(m_z) \begin{pmatrix} \sqrt{I_e/I_\tau} & 0 & 0 \\ 0 & \sqrt{I_\mu/I_\tau} & 0 \\ 0 & 0 & 1 \end{pmatrix} . \quad (3.9)$$

We discuss cases of $\kappa_{33} = 0$ and $\kappa_{11} = \kappa_{22} = \kappa_{33} = 0$ in Appendix B.

Now let us define small parameters of

$$\epsilon_{e,\mu} = 1 - \sqrt{\frac{I_{e,\mu}}{I_\tau}} \quad (3.10)$$

for the later discussions. Figures 1 and 2 show $\tan\beta (= \langle\phi_{\rm u}\rangle/\langle\phi_{\rm d}\rangle)$ dependences of $\epsilon_{e,\mu}$ with $M_R = 10^{13}$GeV and 10^6GeV. They show that magnitudes of $\epsilon_{e,\mu}$ increase as $\tan\beta$ increases. This is because the value of $\sqrt{I_i/I_\tau}$ can be mainly determined by I_τ, and the quantum correction from τ becomes large in the large $\tan\beta$ region¶. We notice that the

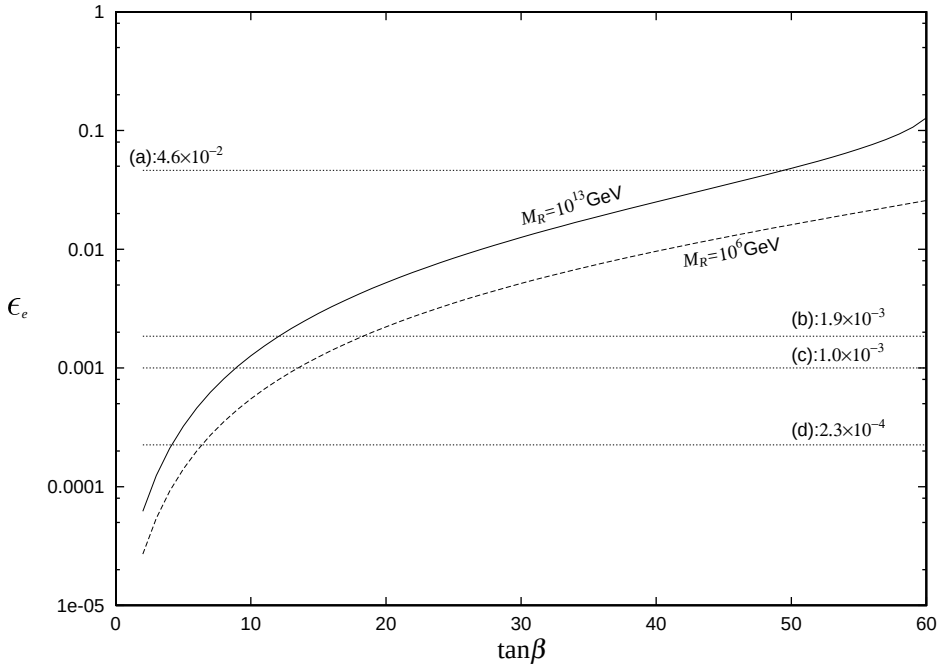

Figure 1: $\tan\beta$ dependence of ϵ_e. Solid-line (dashed-line) shows $M_R = 10^{13}$GeV (10^6GeV). Each dotted-line shows (a):4.6×10^{-2}, (b):1.9×10^{-3}, (c):1.0×10^{-3} and (d):2.3×10^{-4}.

large $\tan\beta$ means large quantum corrections of $\epsilon_{e,\mu}$. Solid-lines (dashed-lines) in Figures 1 and 2 stand for the $\tan\beta$ dependences of $\epsilon_{e,\mu}$ with $M_R = 10^{13}$GeV (10^6GeV). The value of $\epsilon_{e,\mu}$ with $M_R = 10^6$GeV is smaller than that with $M_R = 10^{13}$GeV at the same value of $\tan\beta$. This is because charged-lepton Yukawa couplings are enhanced at the high energy scale. Hereafter, we fix the M_R scale at 10^{13}GeV in our numerical analyses.

¶ We show the approximation of $\sqrt{I_i/I_\tau}$ in Appendix C.

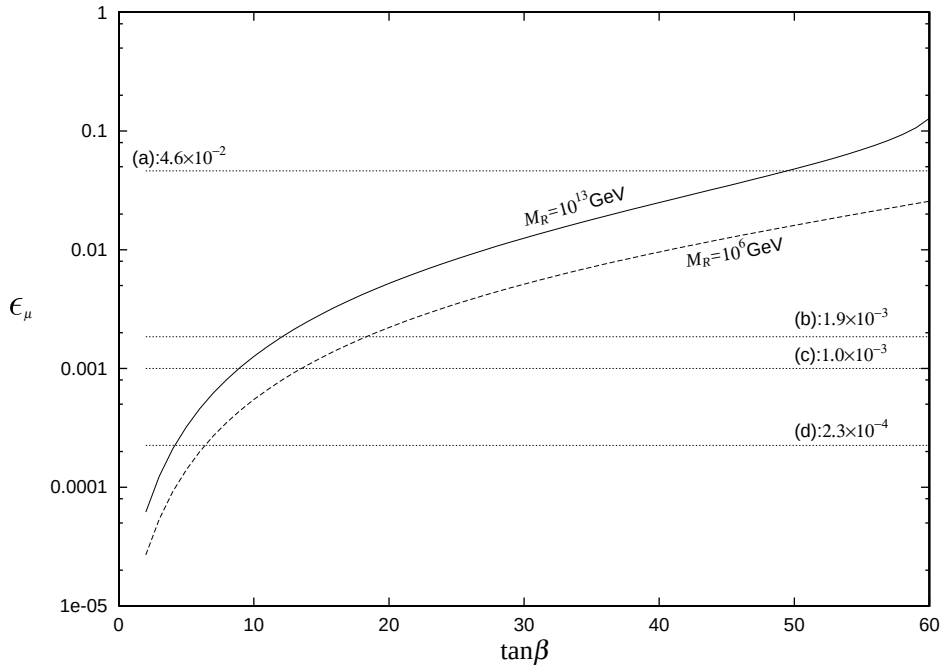

Figure 2: $\tan\beta$ dependence of ϵ_μ. Solid-line (dashed-line) shows $M_R = 10^{13}$GeV (10^6GeV). Each dotted-line shows (a):4.6×10^{-2}, (b):1.9×10^{-3}, (c):1.0×10^{-3} and (d):2.3×10^{-4}.

4 Two Generation Neutrinos

In this section, we neglect the first generation contributions for simplicity, and discuss the stability of the MNS matrix against quantum corrections in the two generation neutrinos.

Neglecting the first generation, eq.(3.9) becomes

$$\kappa(M_R) = \frac{\kappa_{33}(M_R)}{\kappa_{33}(m_z)} \begin{pmatrix} \sqrt{I_\mu/I_\tau} & 0 \\ 0 & 1 \end{pmatrix} \kappa(m_z) \begin{pmatrix} \sqrt{I_\mu/I_\tau} & 0 \\ 0 & 1 \end{pmatrix} . \tag{4.1}$$

We parameterize $\kappa(m_z)$ as

$$\kappa(m_z) = \begin{pmatrix} \cos\theta_{23} & \sin\theta_{23} \\ -\sin\theta_{23} & \cos\theta_{23} \end{pmatrix} \begin{pmatrix} \kappa_2 & 0 \\ 0 & \kappa_3 \end{pmatrix} \begin{pmatrix} \cos\theta_{23} & -\sin\theta_{23} \\ \sin\theta_{23} & \cos\theta_{23} \end{pmatrix} , \tag{4.2}$$

where $\kappa_{2,3}$ are eigenvalues of κ at the m_z scale. From eq.(4.1), the mixing angle at the M_R scale ($\hat{\theta}_{23}$) is given by

$$\tan 2\hat{\theta}_{23} = \frac{\delta k \sin 2\theta_{23}\,(1-\epsilon)}{\delta k \cos 2\theta_{23} + \epsilon\,(2-\epsilon)\left(\kappa_2 + \delta k \sin^2\theta_{23}\right)} , \tag{4.3}$$

where

$$\epsilon \equiv \epsilon_\mu , \quad \text{and} \quad \delta k \equiv \kappa_3 - \kappa_2 . \tag{4.4}$$

Hereafter we denote the mixing angles at the M_R scale as $\hat{\theta}_{ij}$s. Figure 2 shows $0 < \epsilon < 0.15$ for $2 \leq \tan\beta \leq 60$ with $M_R = 10^{13}$ GeV. We notice that $|\delta k|$ is not necessarily smaller than $|\kappa_{2,3}|$, because κ_2 can take the opposite sign of κ_3. We classify the neutrino mass hierarchies into the following three cases as Type A$^{(2)}$: $|\kappa_3| \gg |\kappa_2|$, Type B1$^{(2)}$: $\kappa_3 \simeq \kappa_2$ and Type B2$^{(2)}$: $\kappa_3 \simeq -\kappa_2$. We study the stability of the mixing angle in each case.

(1). Type A$^{(2)}$:

When $|\kappa_2|$ is much smaller than $|\kappa_3|$ (*i.e.,* $\delta k \sim |\kappa_3| \gg |\kappa_2| \simeq 0$), eq.(4.2) becomes

$$\kappa(m_z) \simeq \kappa_3 \cos^2\theta_{23} \begin{pmatrix} \tan^2\theta_{23} & \tan\theta_{23} \\ \tan\theta_{23} & 1 \end{pmatrix} . \tag{4.5}$$

In this case, the mixing angle $\hat{\theta}_{23}$ is given by

$$\tan 2\hat{\theta}_{23} = \frac{\sin 2\theta_{23}(1-\epsilon)}{\cos 2\theta_{23} + \epsilon(2-\epsilon)\sin^2\theta_{23}} = \tan 2\theta_{23}\,(1 - \epsilon \sec 2\theta_{23}) + O(\epsilon^2) \tag{4.6}$$

from eq.(4.3). This means $\hat{\theta}_{23}$ is stable against the quantum correction of ϵ.

(2). Type B1$^{(2)}$:

In the case of $\kappa_2 \simeq \kappa_3$ (*i.e.,* $\kappa_2\kappa_3 > 0,\ 0 < |\delta k| \ll |\kappa_{2,3}|$), $\kappa(m_z)$ is given by

$$\kappa(m_z) = \begin{pmatrix} \kappa_3 - \dfrac{\delta k}{2} & \dfrac{\delta k}{2} \\ \dfrac{\delta k}{2} & \kappa_3 - \dfrac{\delta k}{2} \end{pmatrix} \simeq \left(\kappa_3 - \frac{\delta k}{2}\right) \begin{pmatrix} 1 & \dfrac{\delta k}{2\kappa_3} \\ \dfrac{\delta k}{2\kappa_3} & 1 \end{pmatrix} , \tag{4.7}$$

around the maximal mixing $\theta_{23} = \pi/4$. Let us discuss the stability of eq.(4.7) against the renormalization effects. Equation (4.3) induces the mixing angle $\hat{\theta}_{23}$ as

$$\tan 2\hat{\theta}_{23} \simeq \frac{1}{2\epsilon}\,\frac{\delta k}{\kappa_3} . \tag{4.8}$$

This means the mixing angle of $\hat{\theta}_{23}$ strongly depends on the quantum correction of ϵ. When the value of $\delta k/\kappa_3$ is larger than ϵ, the mixing angle does not receive significant change from renormalization corrections. On the other hand, when $\epsilon > \delta k/\kappa_3$, the mixing angle strongly depends on RGE effects, and the mixing angle at the M_R scale can be small even if the maximal mixing is realized at the m_z scale. This situation has been already discussed in Ref. [19].

(3). Type $B2^{(2)}$:

If the absolute value of $\kappa_{2,3}$ are the same order, but they have opposite signs from each other (*i.e.*, $\kappa_2\kappa_3 < 0$, $|\delta k| \simeq 2|\kappa_{2,3}|$), $\kappa(m_z)$ is given by

$$\kappa(m_z) \simeq \kappa_3 \cos 2\theta_{23} \begin{pmatrix} -1 & \tan 2\theta_{23} \\ \tan 2\theta_{23} & 1 \end{pmatrix} . \tag{4.9}$$

In this case, eq.(4.3) induces

$$\tan 2\hat{\theta}_{23} = \tan 2\theta_{23} \left(\frac{2\,(1-\epsilon)}{2-\epsilon\,(2-\epsilon)} \right) = \tan 2\theta_{23} + O(\epsilon^2)\,. \tag{4.10}$$

This means that the mixing angle is stable against the small change of ϵ.

hierarchy	$\kappa(m_z)$	$\tan 2\hat{\theta}_{23}$(mixing angle at the M_R)	Stability
Type $A^{(2)}$ $(\kappa_3 \gg \kappa_2)$	$\kappa_3 \cos^2\theta_{23} \begin{pmatrix} \tan^2\theta_{23} & \tan\theta_{23} \\ \tan\theta_{23} & 1 \end{pmatrix}$	$\tan 2\theta_{23}\,(1 - \epsilon \sec 2\theta_{23}) + O(\epsilon^2)$	stable
Type $B1^{(2)}$ $(\kappa_3 \simeq \kappa_2)$ $(\theta_{23} = \pi/4)$	$\left(\kappa_3 - \frac{\delta k}{2}\right) \begin{pmatrix} 1 & \frac{\delta k}{2\kappa_3} \\ \frac{\delta k}{2\kappa_3} & 1 \end{pmatrix}$	$\simeq \frac{1}{2\epsilon}\,\frac{\delta k}{\kappa_3}$	unstable $(\epsilon > \frac{\delta k}{\kappa_3})$
Type $B2^{(2)}$ $(\kappa_3 \simeq -\kappa_2)$	$\kappa_3 \cos 2\theta_{23} \begin{pmatrix} -1 & \tan 2\theta_{23} \\ \tan 2\theta_{23} & 1 \end{pmatrix}$	$\tan 2\theta_{23} + O(\epsilon^2)$	stable

Table 1: Stabilities of the two generation case.

Table 1 shows the stability of the MNS matrix in the two generation neutrinos. Mixing angles of Type $A^{(2)}$ and Type $B2^{(2)}$ are stable against the small change of ϵ. This means they are stable against quantum corrections. The mixing angle of Type $B1^{(2)}$ is unstable around $\theta_{23} = \pi/4$ when $\epsilon > \delta k/\kappa_3$. The mixing angle of this case is sensitive to the quantum corrections, and determined from the ratio of $\delta k/\kappa_3$ and ϵ. Table 1 shows that the neutrino mass hierarchy and the relative sign assignment of mass eigenvalues play the crucial roles for the stability of the MNS matrix.

5 Three Generation Neutrinos

Now let us discuss the stability of the MNS matrix in the three generation neutrinos against quantum corrections according to the classification of mass hierarchies in eqs.(1.4).

5.1 Type A

In Type A, the mass spectrum is given by

$$m_1 = 0\,, \quad m_2 = \sqrt{\Delta m^2_{\rm solar}}\,, \quad m_3 = \sqrt{\Delta m^2_{\rm solar} + \Delta m^2_{\rm ATM}}\,. \tag{5.1}$$

Neutrino masses of this type have large hierarchies. In this type, there are following relative sign assignments for mass eigenvalues.

$$\text{case (a1):} \quad m_\nu^{\rm a1} = diag.(0, m_2, m_3) \tag{5.2a}$$

$$\text{case (a2):} \quad m_\nu^{\rm a2} = diag.(0, -m_2, m_3) \tag{5.2b}$$

The neutrino mass matrices at the weak scale for (a1) and (a2) are shown in Table 2, where we write the leading order of each element, and the small parameter ξ_a is defined as

$$\xi_{\rm a} = \frac{m_2}{m_3} \simeq \sqrt{\frac{\Delta m^2_{\rm solar}}{\Delta m^2_{\rm ATM}}}\,. \tag{5.3}$$

The relation between the neutrino mass matrices at m_z and M_R is given by

$$M_\nu(M_R) = \begin{pmatrix} 1-\epsilon_e & 0 & 0 \\ 0 & 1-\epsilon_\mu & 0 \\ 0 & 0 & 1 \end{pmatrix} M_\nu(m_z) \begin{pmatrix} 1-\epsilon_e & 0 & 0 \\ 0 & 1-\epsilon_\mu & 0 \\ 0 & 0 & 1 \end{pmatrix}. \tag{5.4}$$

The mixing angles of the MNS matrix at M_R can be obtained from eq.(5.4). Table 3 shows $\tan\beta$ dependences of the mixing angles at M_R in the region of $2 \le \tan\beta \le 60$. Since $U_{e3} \simeq 0$ from the numerical analysis, the MNS matrix can be regarded as two sets of two generation mixings, which are between the first and the second generations and also between the second and the third generations. Since the large mass hierarchies exist in the first and the second generations and also in the second and the third generations as $m_1 \ll m_2$ and $m_2 \ll m_3$, $\sin^2 2\hat{\theta}_{12}$ and $\sin^2 2\hat{\theta}_{23}$ are also stable against quantum corrections on the analogy of Type A$^{(2)}$. The numerical analyses really show all mixing angles are not changed significantly by quantum corrections. This means that the MNS matrix is stable against quantum corrections in (a1) and (a2).

	neutrino mass matrix up to the leading order	Stability
case(a1) $diag.(0, m_2, m_3)$	$\frac{m_3}{2}\begin{pmatrix} 2\xi_{\rm a}\sin^2\theta & \xi_{\rm a}\sin 2\theta/\sqrt{2} & -\xi_{\rm a}\sin 2\theta/\sqrt{2} \\ \xi_{\rm a}\sin 2\theta/\sqrt{2} & 1 & 1 \\ -\xi_{\rm a}\sin 2\theta/\sqrt{2} & 1 & 1 \end{pmatrix}$	stable
case(a2) $diag.(0, -m_2, m_3)$	$\frac{m_3}{2}\begin{pmatrix} -2\xi_{\rm a}\sin^2\theta & -\xi_{\rm a}\sin 2\theta/\sqrt{2} & \xi_{\rm a}\sin 2\theta/\sqrt{2} \\ -\xi_{\rm a}\sin 2\theta/\sqrt{2} & 1 & 1 \\ \xi_{\rm a}\sin 2\theta/\sqrt{2} & 1 & 1 \end{pmatrix}$	stable

Table 2: Neutrino mass matrices at the weak scale for (a1) and (a2).

		MSW-S	MSW-L	VO
(a1)	$\sin^2 2\hat{\theta}_{12}$	$0.007 \sim 0.006$	$1 \sim 0.996$	$1 \sim 0.996$
	$\sin^2 2\hat{\theta}_{23}$	$1 \sim 0.98$	$1 \sim 0.98$	$1 \sim 0.98$
	$\sin^2 2\hat{\theta}_{13}$	$0.0 \sim 2.7 \times 10^{-7}$	$0.0 \sim 8.8 \times 10^{-5}$	$0.0 \sim 3.7 \times 10^{-10}$
(a2)	$\sin^2 2\hat{\theta}_{12}$	$0.007 \sim 0.006$	$1 \sim 0.996$	$1 \sim 0.996$
	$\sin^2 2\hat{\theta}_{23}$	$1 \sim 0.98$	$1 \sim 0.98$	$1 \sim 0.98$
	$\sin^2 2\hat{\theta}_{13}$	$0.0 \sim 2.2 \times 10^{-7}$	$0.0 \sim 6.8 \times 10^{-5}$	$0.0 \sim 3.7 \times 10^{-10}$

Table 3: $\tan\beta$ dependences of the mixing angles at M_R in (a1) and (a2) ($2 \leq \tan\beta \leq 60$).

5.2 Type B

At first we consider the case that m_1 is larger than m_2. Then the mass spectrum of this type is given by

$$m_1 = \sqrt{\Delta m^2_{\rm ATM} + \Delta m^2_{\rm solar}}\,, \quad m_2 = \sqrt{\Delta m^2_{\rm ATM}}\,, \quad m_3 = 0\,. \tag{5.5}$$

There are following two cases according to the relative sign assignments for masses.

$$\text{case (b1):} \quad m_\nu^{b1} = diag.(m_1, m_2, 0) \tag{5.6a}$$

$$\text{case (b2):} \quad m_\nu^{b2} = diag.(m_1, -m_2, 0) \tag{5.6b}$$

The neutrino mass matrices at m_z for (b1) and (b2) are listed in Table 4, where the small parameter ξ_b is defined as

$$\xi_b = \frac{m_2 - m_1}{m_1} = -\frac{1}{2}\ \frac{\Delta m^2_{\rm solar}}{\Delta m^2_{\rm ATM}}\,. \tag{5.7}$$

	neutrino mass matrix up to the leading order	Stability
case(b1) $diag.(m_1, m_2, 0)$	$\frac{m_1}{2}\begin{pmatrix} 2 & \xi_b \sin 2\theta/\sqrt{2} & -\xi_b \sin 2\theta/\sqrt{2} \\ \xi_b \sin 2\theta/\sqrt{2} & 1 & -1 \\ -\xi_b \sin 2\theta/\sqrt{2} & -1 & 1 \end{pmatrix}$	unstable $(\sin^2 2\theta_{12})$
case(b2) $diag.(m_1, -m_2, 0)$	$-\frac{m_1 \cos 2\theta}{2}\begin{pmatrix} -2 & \sqrt{2}\tan 2\theta & -\sqrt{2}\tan 2\theta \\ \sqrt{2}\tan 2\theta & 1 & -1 \\ -\sqrt{2}\tan 2\theta & -1 & 1 \end{pmatrix}$	stable

Table 4: Neutrino mass matrices at m_z for (b1) and (b2).

We analyze the stability of the MNS matrix for (b1) and (b2) against quantum corrections by using $M_\nu(M_R)$ obtained from eq.(5.4). The results of our numerical analyses are listed in Table 5. Let us see the details in both (b1) and (b2).

		MSW-S	MSW-L	VO
(b1)	$\sin^2 2\hat{\theta}_{12}$	see Figure 3		
	$\sin^2 2\hat{\theta}_{23}$	$1 \sim 0.98$	$1 \sim 0.98$	$1 \sim 0.98$
	$\sin^2 2\hat{\theta}_{13}$	0.0	0.0	0.0
(b2)	$\sin^2 2\hat{\theta}_{12}$	0.007	1	1
	$\sin^2 2\hat{\theta}_{23}$	$1 \sim 0.98$	$1 \sim 0.98$	$1 \sim 0.98$
	$\sin^2 2\hat{\theta}_{13}$	0.0	0.0	0.0

Table 5: $\tan\beta$ dependences of the mixing angles at M_R in (b1) and (b2) ($2 \leq \tan\beta \leq 60$).

case(b1): Eigenvalues of $M_\nu(M_R)$ are given by

$$\begin{aligned} &\overline{m}_1 = m_1(1+\xi_b)\,, \quad \overline{m}_2 = m_1(1-3\epsilon)\,, \quad \overline{m}_3 = 0\,, \quad (|\xi_b| < 3|\epsilon|)\,, \\ &\overline{m}_1 = m_1(1-3\epsilon)\,, \quad \overline{m}_2 = m_1(1+\xi_b)\,, \quad \overline{m}_3 = 0\,, \quad (|\xi_b| > 3|\epsilon|)\,, \end{aligned} \tag{5.8}$$

up to order of ϵ and ξ_b for any value of θ.

Numerical analyses of Table 5 suggest $\sin^2 2\hat{\theta}_{13}$ and $\sin^2 2\hat{\theta}_{23}$ are stable against quantum corrections. This is because there are large hierarchies of $m_1 \ll m_3$ and $m_2 \ll m_3$ on the analogy of Type $A^{(2)}$. How about $\sin^2 2\hat{\theta}_{12}$? Figure 3 shows that $\sin^2 2\hat{\theta}_{12}$ can be changed by quantum corrections according to the solar neutrino solutions.

In the MSW-L solution, $\sin^2 2\hat{\theta}_{12}$ is damping around $\tan\beta \sim 20$. On the other hand , $\sin^2 2\hat{\theta}_{12} \simeq 0$ even in the small $\tan\beta$ region in the VO solution. These situations can be

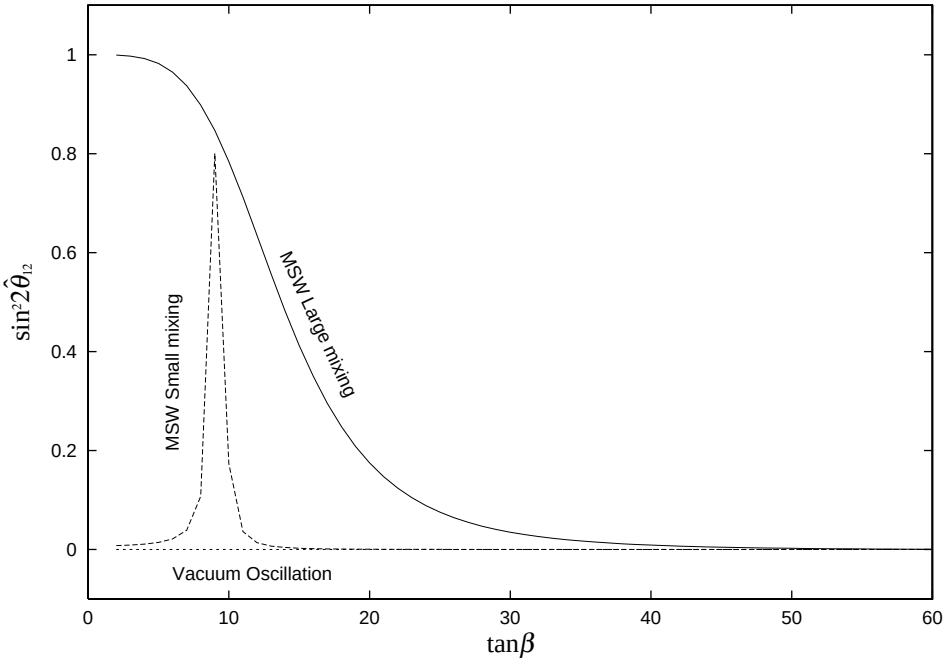

Figure 3: $\tan\beta$ dependences of $\sin^2 2\hat{\theta}_{12}$ according to the solar neutrino solutions in (b1).

easily understood as follows. From eq.(5.4), $\tan 2\hat{\theta}_{12}$ is estimated to be

$$\tan 2\hat{\theta}_{12} \simeq \tan 2\theta_{12} \left(1 - \frac{1}{\cos 2\theta_{12}} \frac{\epsilon}{|\xi_b|}\right)^{-1}, \tag{5.9}$$

where we use the approximation of $\epsilon_e \simeq \epsilon_\mu (\equiv \epsilon)$. When θ_{12} is $\pi/4$, eq.(5.9) becomes

$$\tan 2\hat{\theta}_{12} \simeq \frac{\xi_b}{2\epsilon} \sim \begin{cases} \dfrac{10^{-3}}{\epsilon} & (\text{MSW-L}), \\ \dfrac{10^{-9}}{\epsilon} & (\text{VO}), \end{cases} \tag{5.10}$$

from eq.(5.7). Dotted-lines of (c) in Figures 1 and 2 show that ϵ is much larger than 10^{-3} in the region of $\tan\beta > 20$. Then, from eq.(5.10), $\sin^2 2\hat{\theta}_{12}$ is sufficiently small when $\tan\beta$ is larger than 20 in the MSW-L solution. On the other hand, eq.(5.10) suggests $\sin^2 2\hat{\theta}_{12} \simeq 0$ even in the small $\tan\beta$ region in the VO solution.

In the MSW-S solution, $\sin^2 2\hat{\theta}_{12}$ has a peak around $\tan\beta \sim 10$. When $\theta_{12} \ll 1$, eq.(5.9) becomes

$$\tan 2\hat{\theta}_{12} \simeq 2\theta_{12} \left(1 - \frac{\epsilon}{|\xi_b|}\right)^{-1}. \tag{5.11}$$

This means $\tan 2\hat{\theta}_{12}$ diverges infinity ($\sin^2 2\hat{\theta}_{12} \sim 1$) at $\epsilon \simeq |\xi_b|$. Equation (5.7) suggests $|\xi_b|$ is about 10^{-3}. Figures 1 and 2 show $\epsilon \simeq 10^{-3}$ around $\tan\beta \sim 10$. Thus, $\sin^2 2\hat{\theta}_{12}$ becomes one around $\tan\beta \sim 10$ independently of the value of θ_{12}. This is the reason why the peak in the Figure 3 appears in the MSW-S solution.

Finally, let us see how the stability of the MNS matrix is changed if we take the mass spectrum as

$$m_1 = \sqrt{\Delta m^2_{\rm ATM}}\,, \quad m_2 = \sqrt{\Delta m^2_{\rm ATM} + \Delta m^2_{\rm solar}}\,, \quad m_3 = \sqrt{\Delta m^2_{\rm solar}}\,, \tag{5.12}$$

in stead of eqs.(5.5). In this case, eq.(5.9) becomes

$$\tan 2\hat{\theta}_{12} \simeq 2\theta_{12} \left(1 + \frac{1}{\cos 2\theta_{12}} \frac{\epsilon}{|\xi_b|}\right)^{-1}, \tag{5.13}$$

and eq.(5.7) is replaced by

$$\xi_b = \frac{m_2 - m_1}{m_1} = \frac{1}{2}\frac{\Delta m^2_{solar}}{\Delta m^2_{\rm ATM}}\,. \tag{5.14}$$

The behaviors of the mixing angles against quantum corrections for the MSW-L and the VO solutions are the same as those of eqs.(5.5). As for the MSW-S solution the mixing angle $\hat{\theta}_{12}$ becomes stable against renormalization effects, and the peak of $\sin^2 2\hat{\theta}_{12}$ around $\tan\beta \sim 10$ disappears due to the positive sign of eq.(5.13).

case(b2): Eigenvalues of $M_\nu(M_R)$ are given by

$$\begin{aligned}
\overline{m}_1 &= m_1 \left(\sqrt{1 + \xi_b - 3\epsilon} + \frac{1}{2}\left(\xi_b + \epsilon\cos 2\theta\right)\right), \\
\overline{m}_2 &= -m_1 \left(\sqrt{1 + \xi_b - 3\epsilon} - \frac{1}{2}\left(\xi_b + \epsilon\cos 2\theta\right)\right), \\
\overline{m}_3 &= 0\,,
\end{aligned} \tag{5.15}$$

up to order of ϵ and ξ_b. Numerical analyses of Table 5 show the MNS matrix is stable against quantum corrections. This can be easily understood as follows. $\sin^2 2\hat{\theta}_{13}$ and $\sin^2 2\hat{\theta}_{23}$ are stable against quantum corrections, because there are large hierarchies between the first and the third generations and also between the second and the third generations on the analogy of Type $A^{(2)}$. $\sin^2 2\hat{\theta}_{12}$ is also stable against the renormalization effects, since the signs of m_1 and m_2 are different from each other on the analogy of Type $B2^{(2)}$. Thus, we can conclude all $\sin^2 2\theta_{ij}$s are stable against renormalization effects in case (b2).

5.3 Type C

The mass spectrum is given by

$$m_1 = m_0\,, \quad m_2 = \sqrt{m_0^2 + \Delta m^2_{\rm solar}}\,, \quad m_3 = \sqrt{m_0^2 + \Delta m^2_{\rm solar} + \Delta m^2_{\rm ATM}}\,, \tag{5.16}$$

where m_0 is the degenerate mass scale. We take $m_0 = 1.0$ eV or 0.2 eV in this article. There are following four different cases according to the relative sign assignments of neutrino mass eigenvalues.

$$\text{case (c1):} \quad m_\nu^{c1} = diag.(-m_1, m_2, m_3) \tag{5.17a}$$
$$\text{case (c2):} \quad m_\nu^{c2} = diag.(m_1, -m_2, m_3) \tag{5.17b}$$
$$\text{case (c3):} \quad m_\nu^{c3} = diag.(-m_1, -m_2, m_3) \tag{5.17c}$$
$$\text{case (c4):} \quad m_\nu^{c4} = diag.(m_1, m_2, m_3) \tag{5.17d}$$

We define the small parameters

$$\delta_c \equiv \frac{m_3 - m_2}{m_0} \simeq \frac{1}{2}\frac{\Delta m^2_{\rm ATM}}{m_0^2}\,, \quad \text{and} \quad \xi_c \equiv \frac{m_2 - m_1}{m_0} \simeq \frac{1}{2}\frac{\Delta m^2_{\rm solar}}{m_0^2}\,, \tag{5.18}$$

where ξ_c is always smaller than δ_c. The neutrino mass matrices for all types are listed in Table 6 up to the leading order for each element.

In the case of $m_0 = 1.0$ eV all solar neutrino solutions of (c3) and (c4), and the MSW-S solution of (c1) and (c2) are excluded by the neutrino-less double-β decay experiments [20], whose upper limit is given by $\langle m_{\nu_e}\rangle < 0.2$ eV [21], where

$$\langle m_{\nu_e}\rangle = \left|\sum_{i=1}^{3} m_i \left(V_{\rm MNS}\right)^2_{ei}\right| = \begin{cases} m_0\left(1 + \xi_c \sin^2\theta\right)\,, & (m_1 m_2 > 0)\,, \\ \\ m_0\left(\cos 2\theta - \xi_c \sin^2\theta\right)\,, & (m_1 m_2 < 0)\,, \end{cases} \tag{5.19}$$

from eqs.(2.16) and (5.18). Thus we analyze the stability of the MNS matrix for (c1) and (c2) with $m_0 = 1.0$ eV, and for all cases with $m_0 = 0.2$ eV.

5.3.1 $m_0 = 1.0$ eV

Figures 4 show the $\tan\beta$ dependences of $\sin^2 2\hat{\theta}_{ij}$ in (c1) and (c2) with $m_0 = 1.0$ eV. They shows that all $\sin^2 2\hat{\theta}_{ij}$s gradually approach to the fixed values as $\tan\beta$ becomes large. We can estimate the value of $\tan\beta$ where the mixing angles become close to the fixed values.

Dotted-lines of (b) in Figures 1 and 2 show the value of

$$\delta_c = \frac{\Delta m^2_{\rm ATM}}{2m_0^2} = 1.9 \times 10^{-3}\,, \qquad (m_0 = 1.0 \text{ eV})\,. \tag{5.20}$$

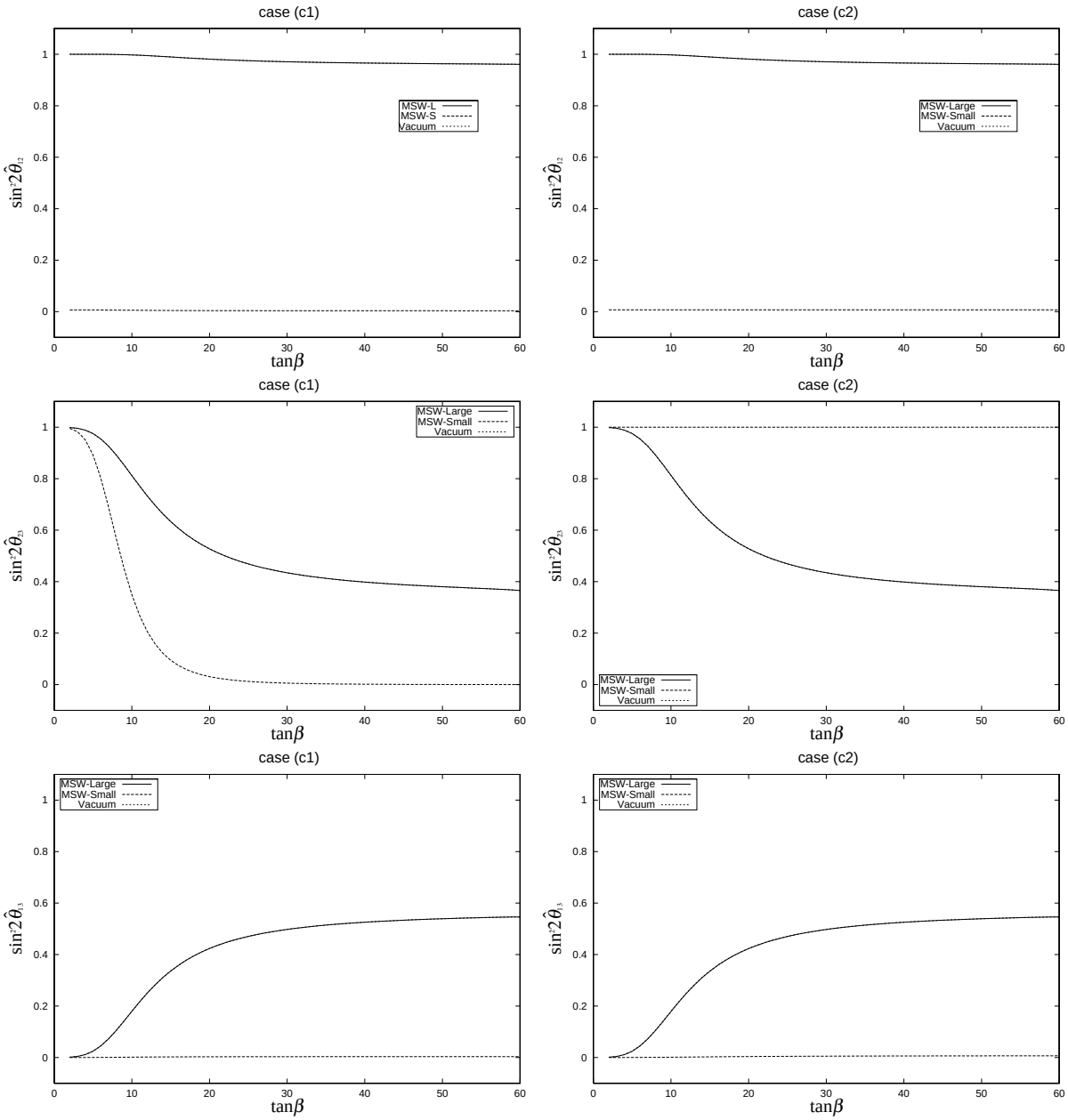

Figure 4: $\tan\beta$ dependences of $\sin^2 2\hat{\theta}_{ij}$ in (c1) and (c2) with $m_0 = 1.0$ eV.

	neutrino mass matrix up to the leading order	Stability
case(c1) $diag.(-m_1, m_2, m_3)$	$\frac{m_0}{2}\begin{pmatrix} -2\cos 2\theta & \sqrt{2}\sin 2\theta & -\sqrt{2}\sin 2\theta \\ \sqrt{2}\sin 2\theta & 1+\cos 2\theta & 1-\cos 2\theta \\ -\sqrt{2}\sin 2\theta & 1-\cos 2\theta & 1+\cos 2\theta \end{pmatrix}$	rearrangement between V_2 and V_3
case(c2) $diag.(m_1, -m_2, m_3)$	$\frac{m_0}{2}\begin{pmatrix} 2\cos 2\theta & -\sqrt{2}\sin 2\theta & \sqrt{2}\sin 2\theta \\ -\sqrt{2}\sin 2\theta & 1-\cos 2\theta & 1+\cos 2\theta \\ \sqrt{2}\sin 2\theta & 1+\cos 2\theta & 1-\cos 2\theta \end{pmatrix}$	rearrangement between V_1 and V_3
case(c3) $diag.(-m_1, -m_2, m_3)$	$m_0\begin{pmatrix} -1 & -\sqrt{2}\xi_c\sin 2\theta & \sqrt{2}\xi_c\sin 2\theta \\ -\sqrt{2}\xi_c\sin 2\theta & \delta_c/2 & 1 \\ \sqrt{2}\xi_c\sin 2\theta & 1 & \delta_c/2 \end{pmatrix}$	rearrangement between V_1 and V_2
case(c4) $diag.(m_1, m_2, m_3)$	$m_0\begin{pmatrix} 1 & \sqrt{2}\xi_c\sin 2\theta & -\sqrt{2}\xi_c\sin 2\theta \\ \sqrt{2}\xi_c\sin 2\theta & 1 & \delta_c/2 \\ -\sqrt{2}\xi_c\sin 2\theta & \delta_c/2 & 1 \end{pmatrix}$	unstable go to the unit matrix

Table 6: Neutrino mass matrices at m_z for (c1) $\sim$ (c4).

We can see that $\delta_c \ll \epsilon$ for $20 \leq \tan\beta$ in Figures 1 and 2. As $\tan\beta$ increases, the quantum effects become larger than the effects of mass squared differences of neutrinos. All $\sin^2 2\hat{\theta}_{ij}$s approach to their fixed values around $\tan\beta \sim 20$ as are shown in Figures 4.

By taking the limit of $\delta_c \ll \epsilon$ we can obtain the fixed values of $\sin^2 2\hat{\theta}_{ij}$ according to the solar neutrino solutions in (c1) and (c2) as follows.

case (c1): The eigenvectors $V_{1,2,3}$ at the m_z scale are given by

$$V_1 = \begin{pmatrix} \cos\theta \\ \frac{-1}{\sqrt{2}}\sin\theta \\ \frac{1}{\sqrt{2}}\sin\theta \end{pmatrix}, \quad V_2 = \begin{pmatrix} \sin\theta \\ \frac{1}{\sqrt{2}}\cos\theta \\ \frac{-1}{\sqrt{2}}\cos\theta \end{pmatrix}, \quad V_3 = \begin{pmatrix} 0 \\ \frac{1}{\sqrt{2}} \\ \frac{1}{\sqrt{2}} \end{pmatrix}. \tag{5.21}$$

V_i is the eigenvector of the i-th eigenvalue of the neutrino mass matrix, which corresponds to each column of the MNS matrix in eq.(2.16). At the M_R scale, eigenvalues of eq.(5.4) are given by

$$m_1(M_R) = -m_0(1 - \epsilon(1 + \cos^2\theta)),$$

$$m_2(M_R) = m_0(1-2\epsilon)\,,$$
$$m_3(M_R) = m_0(1-\epsilon\sin^2\theta)\,, \tag{5.22}$$

up to the order ϵ under the condition of $\delta_c \ll \epsilon$. Eigenvectors of them are given by

$$V_1' = \begin{pmatrix} \cos\theta \\ -\dfrac{\sin\theta}{\sqrt{2}} \\ \dfrac{\sin\theta}{\sqrt{2}} \end{pmatrix}, \quad V_2' = \begin{pmatrix} \dfrac{\sin\theta}{\sqrt{1+\cos^2\theta}} \\ \dfrac{\sqrt{2}\cos\theta}{\sqrt{1+\cos^2\theta}} \\ 0 \end{pmatrix}, \quad V_3' = \begin{pmatrix} -\dfrac{1}{2}\dfrac{\sin 2\theta}{\sqrt{1+\cos^2\theta}} \\ \dfrac{1}{\sqrt{2}}\dfrac{\sin^2\theta}{\sqrt{1+\cos^2\theta}} \\ \dfrac{1}{\sqrt{2}}\sqrt{1+\cos^2\theta} \end{pmatrix}. \tag{5.23}$$

By comparing eq.(5.21) with eq.(5.23), the relation between V_i and V_i' is given as

$$\begin{pmatrix} V_1' \\ V_2' \\ V_3' \end{pmatrix} = \begin{pmatrix} 1 & 0 & 0 \\ 0 & \dfrac{1}{\sqrt{1+\cos^2\theta}} & \dfrac{\cos\theta}{\sqrt{1+\cos^2\theta}} \\ 0 & \dfrac{-\cos\theta}{\sqrt{1+\cos^2\theta}} & \dfrac{1}{\sqrt{1+\cos^2\theta}} \end{pmatrix} \begin{pmatrix} V_1 \\ V_2 \\ V_3 \end{pmatrix}. \tag{5.24}$$

When we take $\pi/4$ (0) for the parameter θ in eq.(5.24), we can obtain the relation between V_i and V_i' for the MSW-L and the VO solutions (the MSW-S solution).

For the MSW-L and the VO solutions, the MNS matrix at the M_R scale is given by

$$\hat{U}_{\rm MNS} = \begin{pmatrix} 1/\sqrt{2} & 1/\sqrt{3} & -1/\sqrt{6} \\ -1/2 & 2/\sqrt{3} & 1/2\sqrt{3} \\ 1/2 & 0 & \sqrt{3}/2 \end{pmatrix} \tag{5.25}$$

in the limit of $\delta_c \ll \epsilon$. The relation between V_i and V_i' is given by

$$V_1' = V_1\,, \qquad V_2' = \sqrt{\frac{2}{3}}\,V_2 + \sqrt{\frac{1}{3}}\,V_3\,, \qquad V_3' = -\sqrt{\frac{1}{3}}\,V_2 + \sqrt{\frac{2}{3}}\,V_3\,. \tag{5.26}$$

For the MSW-S solution[‖], the MNS matrix at the M_R is given by

$$\hat{U}_{\rm MNS} = \begin{pmatrix} 1 & 0 & 0 \\ 0 & 1 & 0 \\ 0 & 0 & 1 \end{pmatrix}, \tag{5.27}$$

which means

$$V_1' = V_1\,, \qquad V_2' = \frac{1}{\sqrt{2}}\,V_2 + \frac{1}{\sqrt{2}}\,V_3\,, \qquad V_3' = -\frac{1}{\sqrt{2}}\,V_2 + \frac{1}{\sqrt{2}}\,V_3\,. \tag{5.28}$$

case (c2): By the same calculations as those of (c1), eigenvalues of eq.(5.4) are obtained as

$$\begin{aligned} m_1(M_R) &= m_0(1-2\epsilon)\,, \\ m_2(M_R) &= -m_0(1-\epsilon(1+\sin^2\theta))\,, \\ m_3(M_R) &= m_0(1-\epsilon\cos^2\theta)\,, \end{aligned} \tag{5.29}$$

up to the $O(\epsilon)$ in $\delta_c \ll \epsilon$. Eigenvectors of them are given by

$$V_1' = \begin{pmatrix} \dfrac{\cos\theta}{\sqrt{1+\sin^2\theta}} \\ -\dfrac{\sqrt{2}\sin\theta}{\sqrt{1+\sin^2\theta}} \\ 0 \end{pmatrix}, \quad V_2' = \begin{pmatrix} \sin\theta \\ \dfrac{\cos\theta}{\sqrt{2}} \\ -\dfrac{\cos\theta}{\sqrt{2}} \end{pmatrix}, \quad V_3' = \begin{pmatrix} \dfrac{1}{2}\dfrac{\sin 2\theta}{\sqrt{1+\sin^2\theta}} \\ \dfrac{1}{\sqrt{2}}\dfrac{\cos^2\theta}{\sqrt{1+\sin^2\theta}} \\ \dfrac{1}{\sqrt{2}}\sqrt{1+\sin^2\theta} \end{pmatrix}. \tag{5.30}$$

By comparing eq.(5.21) with eq.(5.30), the relation between V_i and V_i' is given by

$$\begin{pmatrix} V_1' \\ V_2' \\ V_3' \end{pmatrix} = \begin{pmatrix} \dfrac{1}{\sqrt{1+\sin^2\theta}} & 0 & \dfrac{-\sin\theta}{\sqrt{1+\sin^2\theta}} \\ 0 & 1 & 0 \\ \dfrac{\sin\theta}{\sqrt{1+\sin^2\theta}} & 0 & \dfrac{1}{\sqrt{1+\sin^2\theta}} \end{pmatrix} \begin{pmatrix} V_1 \\ V_2 \\ V_3 \end{pmatrix}. \tag{5.31}$$

[‖] Although the MSW-S solution in (c1) and (c2) with $m_0 = 1.0$ eV is already excluded by the neutrinoless double-β decay experiments of eq.(5.19), we discuss it here to check whether our analytic calculations are consistent with our numerical results or not. We will see they are consistent with each other soon.

For the MSW-L and the VO solutions, the MNS matrix at the M_R scale is given by

$$\hat{U}_{\rm MNS} = \begin{pmatrix} 1/\sqrt{3} & 1/\sqrt{2} & 1/\sqrt{6} \\ -\sqrt{2/3} & 1/2 & 1/2\sqrt{3} \\ 0 & -1/2 & \sqrt{3}/2 \end{pmatrix} \tag{5.32}$$

in $\delta_c \ll \epsilon$. This means

$$V_2' = V_2\,, \qquad V_1' = \sqrt{\frac{2}{3}}\,V_1 - \sqrt{\frac{1}{3}}\,V_3\,, \qquad V_3' = \sqrt{\frac{1}{3}}\,V_1 + \sqrt{\frac{2}{3}}\,V_3\,. \tag{5.33}$$

This is consistent with the results in Ref. [22].

For the MSW-S solution[‖], the MNS matrix at the M_R scale is obtained as

$$\hat{U}_{\rm MNS} = \begin{pmatrix} 1 & 0 & 0 \\ 0 & 1/\sqrt{2} & 1/\sqrt{2} \\ 0 & -1\sqrt{2} & 1/\sqrt{2} \end{pmatrix}, \tag{5.34}$$

which suggests

$$V_1' = V_1\,, \qquad V_2' = V_2\,, \qquad V_3' = V_3\,. \tag{5.35}$$

For the MSW-L and the VO solutions in (c1) and (c2), eqs.(5.25) and (5.32) suggest the fixed values of the $\sin^2 2\hat{\theta}_{ij}$s are

$$\sin^2 2\hat{\theta}_{12} = 0.96\,, \quad \sin^2 2\hat{\theta}_{23} = 0.36\,, \quad \sin^2 2\hat{\theta}_{13} = \frac{5}{9}\,, \tag{5.36}$$

in the limit of $\epsilon \gg \delta_c$. We cannot see the differences between the MSW-L and the VO solutions in Figures 4. It is because the value of $\tan\beta$ where all $\sin^2 2\hat{\theta}_{ij}$s approach to their fixed values are determined by ϵ and δ_c which does not relate to $\Delta m^2_{\rm solar}$ but to $\Delta m^2_{\rm ATM}$. The rearrangements are occurred between V_2 and V_3 in (c1), and V_1 and V_3 in (c2), where the squared mass differences of their eigen values are mainly determined by $\Delta m^2_{\rm ATM}$. On the other hand, for the MSW-S solution eqs.(5.27) and (5.34) suggest all mixing angles approach to zero in the case of (c1), and $\sin^2 2\hat{\theta}_{12} = \sin^2 2\hat{\theta}_{13} = 0$, $\sin^2 2\hat{\theta}_{23} = 1$ in the case of (c2). These results from analytic calculations are completely consistent with those from the numerical analyses as shown in Figure 4.

5.3.2 $m_0 = 0.2$ eV

Figures 5, 6, 7 and 8 show the $\tan\beta$ dependences of $\sin^2 2\hat{\theta}_{ij}$s with $m_0 = 0.2$ eV in (c1), (c2), (c3) and (c4), respectively.

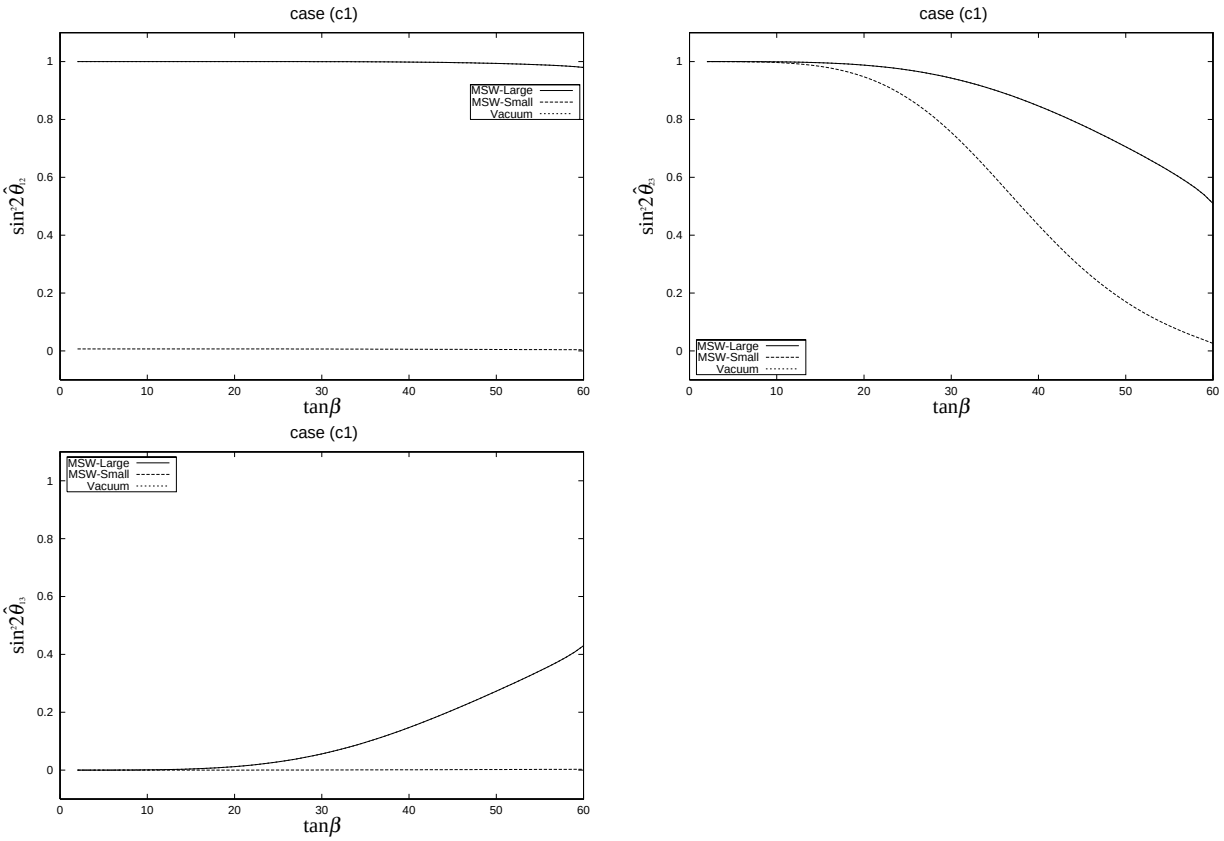

Figure 5: $\tan\beta$ dependences of $\sin^2 2\hat{\theta}_{ij}$ in (c1) with $m_0 = 0.2$ eV.

cases (c1) and (c2): Figures 5 and 6 show that all $\sin^2 2\hat{\theta}_{ij}$s approach to the same fixed values as those with $m_0 = 1.0$ eV in the large $\tan\beta$ region. However, the value of $\tan\beta$ where $\sin^2 2\hat{\theta}_{ij}$s becomes close to their fixed values with $m_0 = 0.2$ eV is larger than that with $m_0 = 1.0$ eV. The value of δ_c with $m_0 = 0.2$ eV is given by

$$\delta_c = \frac{\Delta m^2_{\rm ATM}}{2m_0^2} = 4.6 \times 10^{-2}\,, \qquad (m_0 = 0.2 \text{ eV})\,, \tag{5.37}$$

which is shown as dotted-lines of (a) in Figures 1 and 2. In the region of $2 \leq \tan\beta < 50$, ϵ is not larger than δ_c, and the first (second) generation cannot be regarded to be degenerate with the third generation. Thus, the rearrangement between the eigenvectors of $V_1(V_2)$ and V_3 is not realized completely although the sign of $m_1(m_2)$ is the same as that of m_3. On the other hands, the rearrangement between these eigenvectors is realized with $m_0 = 1.0$ eV in the region of $\tan\beta \geq 20$, where ϵ is already larger than δ_c.

case (c3): Figures 7 show that for all solar neutrino solutions $\sin^2 2\hat{\theta}_{12}$ and $\sin^2 2\hat{\theta}_{13}$ are almost zero in the region of $\tan\beta \geq 10$, and $\sin^2 2\hat{\theta}_{23} \simeq 1$ in all $\tan\beta$ region. Up to the $O(\epsilon)$ eigenvalues of eq.(5.4) are given by

$$m_1(M_R) = -m_0(1 - 2\epsilon)\,,$$

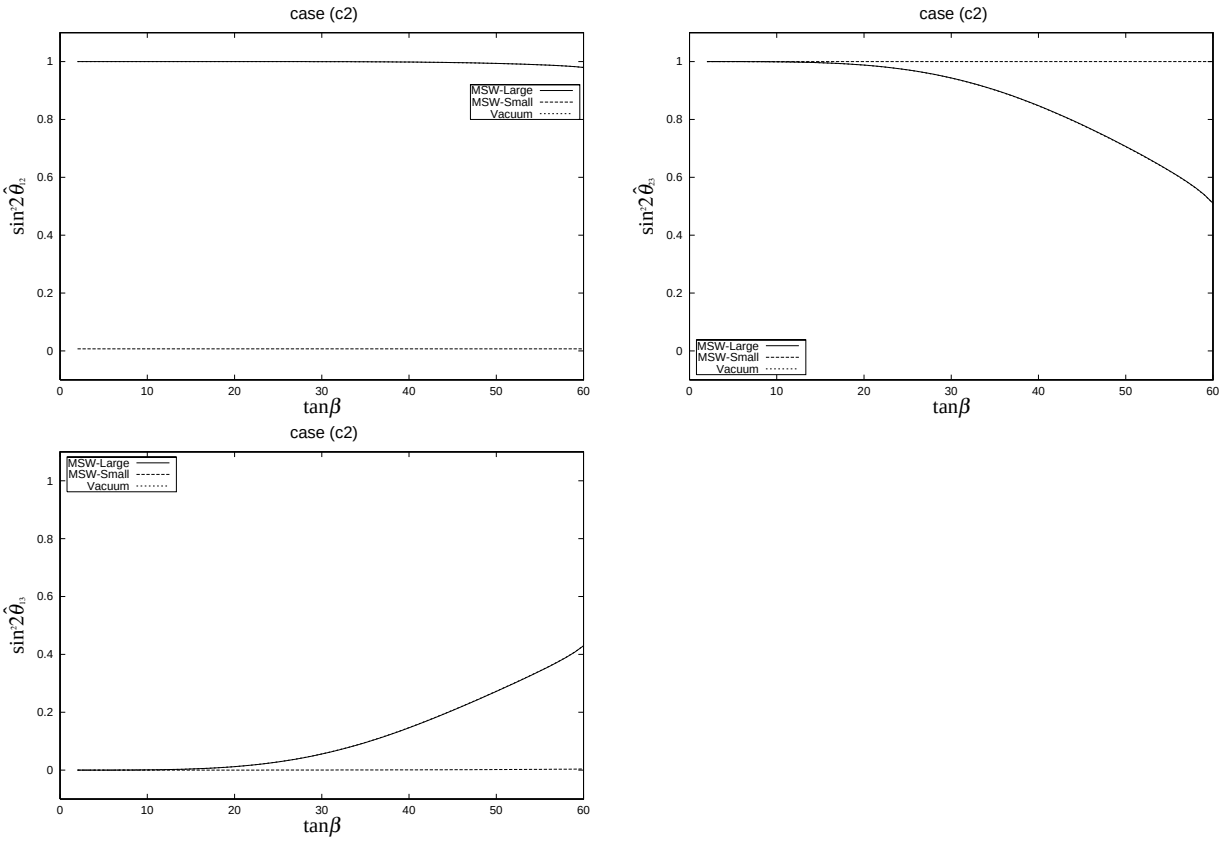

Figure 6: $\tan\beta$ dependences of $\sin^2 2\hat{\theta}_{ij}$ in (c2) with $m_0 = 0.2$ eV.

$$
\begin{aligned}
m_2(M_R) &= -m_0(1-\epsilon)\,, \\
m_3(M_R) &= m_0(1-\epsilon)\,,
\end{aligned}
\tag{5.38}
$$

and eigenvectors of them are given by

$$
V_1' = \begin{pmatrix} 1 \\ 0 \\ 0 \end{pmatrix}, \quad V_2' = \begin{pmatrix} 0 \\ 1/\sqrt{2} \\ -1/\sqrt{2} \end{pmatrix}, \quad V_3' = \begin{pmatrix} 0 \\ 1/\sqrt{2} \\ 1/\sqrt{2} \end{pmatrix}. \tag{5.39}
$$

These eigenvectors and eigenvalues do not depend on the mixing angle θ. Equations (5.39) suggest

$$
\sin^2 2\hat{\theta}_{12} = 0\,, \qquad \sin^2 2\hat{\theta}_{23} = 1\,, \qquad \sin^2 2\hat{\theta}_{13} = 0\,, \tag{5.40}
$$

from eqs.(2.7) in the region of $\xi_c \ll \epsilon$. By comparing eq.(5.21) with eq.(5.39), we can obtain

$$
\begin{pmatrix} V_1' \\ V_2' \\ V_3' \end{pmatrix} = \begin{pmatrix} \cos\theta & \sin\theta & 0 \\ -\sin\theta & \cos\theta & 0 \\ 0 & 0 & 1 \end{pmatrix} \begin{pmatrix} V_1 \\ V_2 \\ V_3 \end{pmatrix}. \tag{5.41}
$$

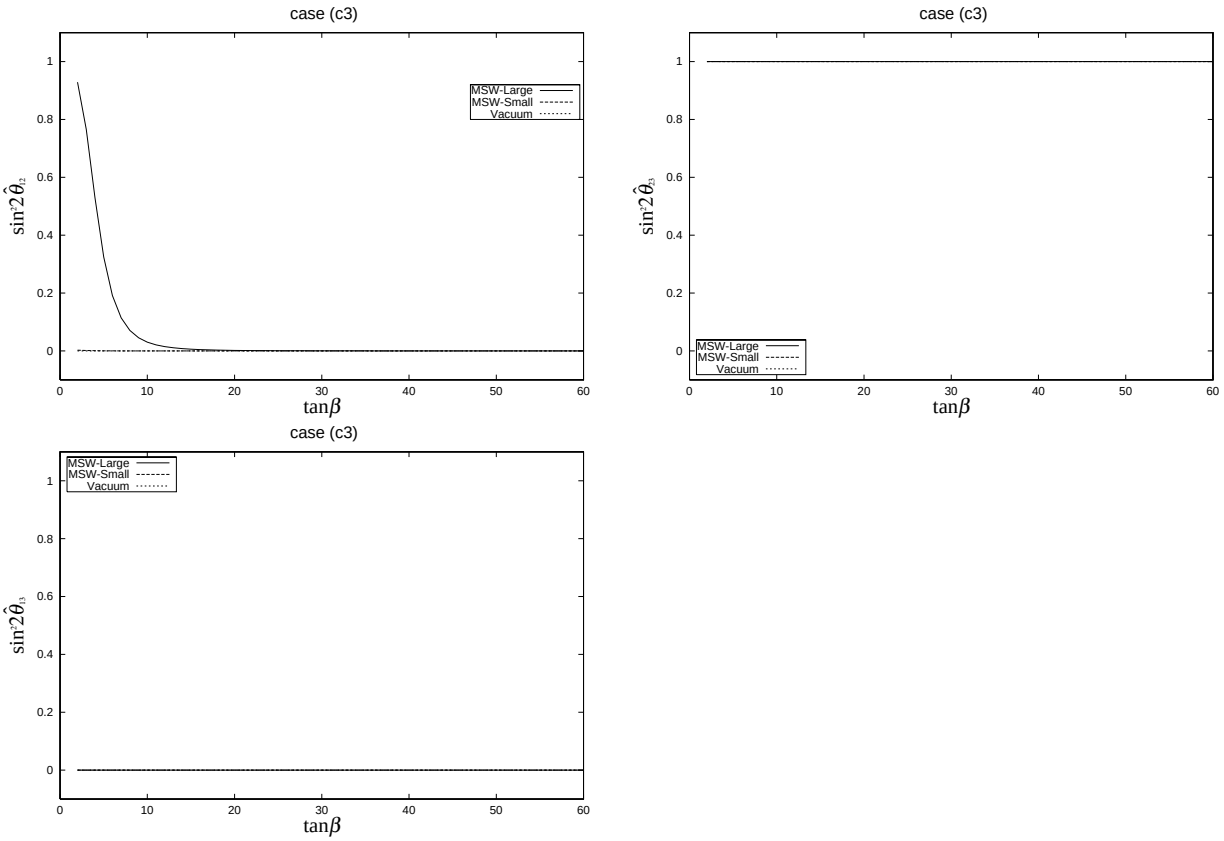

Figure 7: $\tan\beta$ dependences of $\sin^2 2\hat{\theta}_{ij}$ in (c3) with $m_0 = 0.2$ eV.

The rearrangement between V_1 and V_2 is realized, because the sign of m_1 is the same as that of m_2.

Figures 7 show $\sin^2 2\theta_{13}$ and $\sin^2 2\theta_{23}$ are not changed against quantum corrections, and $\sin^2 2\hat{\theta}_{12}$ is close to zero in $\tan\beta \geq 10$ for the MSW-L solution, while $\sin^2 2\hat{\theta}_{12} \simeq 0$ in all $\tan\beta$ region for the VO solution. These situations can be explained by estimating the value of $\tan\beta$ where the mixing angles are close to the fixed values. For the MSW-L solution, the value of ξ_c is given by

$$\xi_c = \frac{\Delta m^2_{\rm MSW-L}}{2m_0^2} = 2.3 \times 10^{-4}\,. \tag{5.42}$$

which is shown as dotted-lines of (d) in Figures 1 and 2. Since ξ_c is much smaller than ϵ in the region of $10 \leq \tan\beta$, the first and the second generations are regarded to be degenerate at m_0, and the rearrangement between V_1 and V_2 is realized. On the other hand, the VO solution gives the value of ξ_c as

$$\xi_c = \frac{\Delta m^2_{\rm VO}}{2m_0^2} = 1.1 \times 10^{-9}\,, \tag{5.43}$$

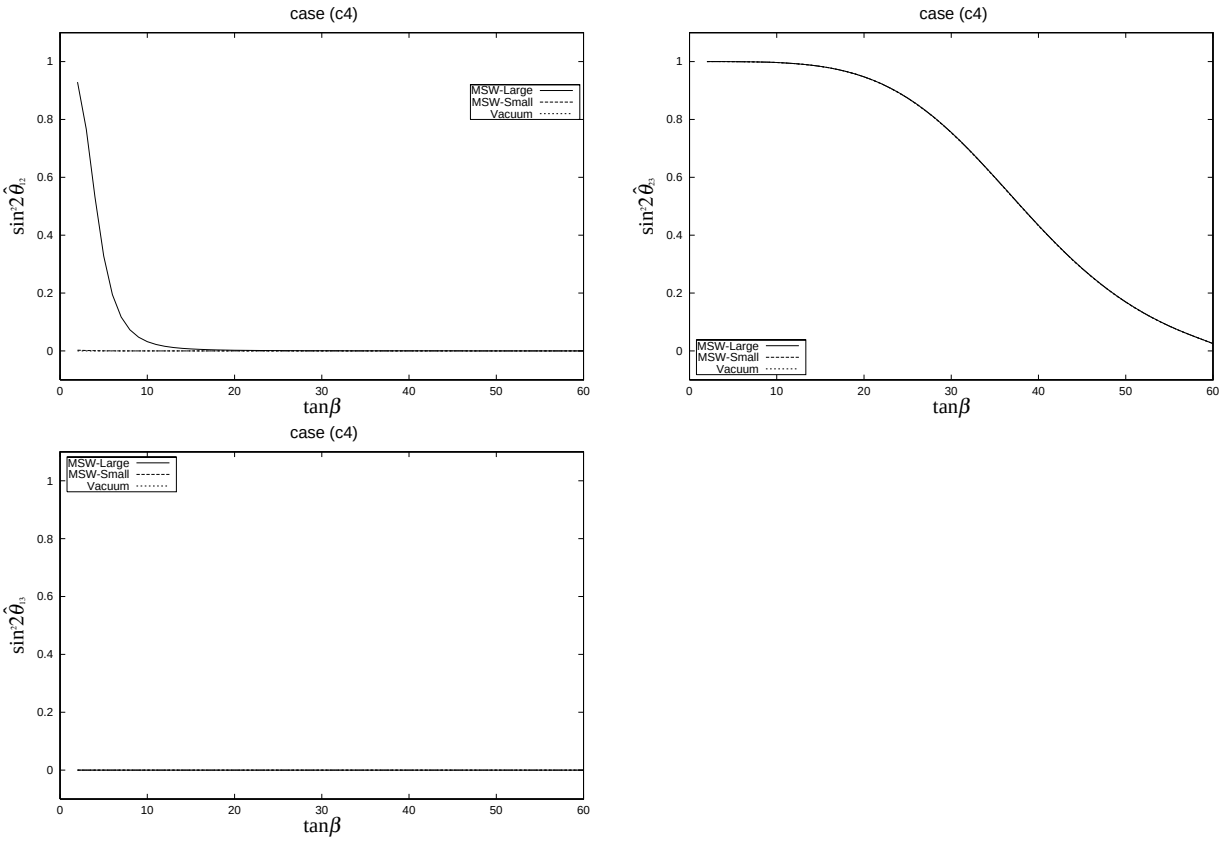

Figure 8: $\tan\beta$ dependences of $\sin^2 2\hat{\theta}_{ij}$ in (c4) with $m_0 = 0.2$ eV.

which is much smaller than ϵ in all $\tan\beta$ region. Therefor the rearrangement between V_1 and V_2 is realized even in the small $\tan\beta$ region for the VO solution.

case (c4): Figures 8 show all $\sin^2 2\hat{\theta}_{ij}$s approach to zero in the large $\tan\beta$ region. This means the MNS matrix becomes the unit matrix in the limit of $\epsilon \gg \delta_c$. In the case of (c4) we cannot obtain the rearrangement rule between V_i and V_i', because κ becomes proportional to the unit matrix which can be diagonalized by any unitary matrices.

Let us see the MSW-L solution at first. Figures 1 and 2 show $\xi_c \ll \delta_c \sim \epsilon$ in the region of $10 < \tan\beta < 50$, where the value of ξ_c (δ_c) is shown in eq.(5.42) (eq.(5.37)). In this region eq.(5.4) becomes

$$M_\nu(M_R) \simeq m_0 \begin{pmatrix} 1-2\epsilon & 0 & 0 \\ 0 & (1-2\epsilon) & (1-\epsilon)\,\delta_c/2 \\ 0 & (1-\epsilon)\,\delta_c/2 & 1 \end{pmatrix}. \tag{5.44}$$

This means $\sin^2 2\hat{\theta}_{12}$ approaches to zero in $10 < \tan\beta$. Equation (5.44) also suggests the mixing between the second and the third generations as

$$\tan 2\hat{\theta}_{23} \simeq \frac{\delta_c}{2\epsilon}\,. \tag{5.45}$$

In $\tan\beta > 50$, ϵ is larger than δ_c, and $\sin^2 2\hat{\theta}_{23}$ becomes small as we can see in Figures 8.

For the VO solution, since the value of ξ_c in eq.(5.43) is much smaller than values of ϵ and δ_c, $M_\nu(M_R)$ also becomes eq.(5.44) in all $\tan\beta$ region. Therefor, $\sin^2 2\hat{\theta}_{12}$ and $\sin^2 2\hat{\theta}_{13}$ are zero at any value of $\tan\beta$. The behavior of $\sin^2 2\hat{\theta}_{23}$ in the VO solution is the same as that in the MSW-L solution, since eq.(5.44) is independent of ξ_c.

Since the mixing angle $\theta \simeq 0$ for the MSW-S solution, $M_\nu(M_R)$ also becomes eq.(5.44). Thus $\sin^2 2\hat{\theta}_{12}$ and $\sin^2 2\hat{\theta}_{13}$ are zero in all $\tan\beta$ region, and $\tan\beta$ dependence of $\sin^2 2\hat{\theta}_{23}$ is the same as that in the MSW-L (VO) solution.

6 Conclusion

In this article, we study the stability of the Maki-Nakagawa-Sakata (MNS) lepton-flavor mixing matrix against quantum corrections in the minimal supersymmetric Standard Model (MSSM) with effective dimension-five operators which give Majorana masses of neutrinos. We decide parameters of the MNS matrix at the weak scale from the data of experiments, and obtain the MNS matrix at the high-energy scale by calculating the quantum corrections. Then we analyze the stability of the MNS matrix at the high energy scale according to types of neutrino mass hierarchy.

In the two generation neutrinos, the mixing angles of Type $A^{(2)}$ ($\kappa_3 \gg \kappa_2$) and Type $B2^{(2)}$ ($\kappa_3 \simeq -\kappa_2$) are stable against quantum corrections, where κ_is are eigenvalues of 2×2 neutrino mass matrix at the weak scale. The mixing angle of Type $B1^{(2)}$ ($\kappa_3 \simeq \kappa_2$) is unstable around $\theta_{23} = \pi/4$ when the magnitude of the quantum correction ϵ is larger than that of $\delta k/\kappa_3$.

In the three generation neutrinos, the stability of the MNS matrix strongly depends on the types of mass hierarchy and the relative sign assignments of mass eigenvalues. The results are obtained as follows.

(1). Type A ($m_1 \sim m_2 \ll m_3$)

The MNS matrix is stable against quantum corrections.

(2). Type B ($m_1 \sim m_2 \gg m_3$)

$\sin^2 2\theta_{13}$ and $\sin^2 2\theta_{23}$ are stable against quantum corrections because there are large hierarchies between the first and the third generations and also between the second and the third generations on the analogy of Type $A^{(2)}$,

<u>case (b1)</u>: $diag(m_1, m_2, 0)$

$\sin^2 2\theta_{12}$ is unstable against quantum corrections. This is understood on the analogy of Type $B1^{(2)}$. Thus, the MNS matrix is unstable against quantum corrections.

case (b2): $diag(m_1, -m_2, 0)$

$\sin^2 2\hat{\theta}_{12}$ is also stable against quantum corrections analogous to the case of Type $B2^{(2)}$. The MNS matrix is stable against quantum corrections.

(3). Type C ($m_1 \sim m_2 \sim m_3$)

The MNS matrix approaches to the definite unitary matrix according to the relative sign assignments of neutrino mass eigenvalues, as the effects of quantum corrections become large enough to neglect squared mass differences of neutrinos. Independent parameters of the MNS matrix at the M_R scale approach to the following fixed values in the large limit of quantum corrections.

case (c1): $diag.(-m_1, m_2, m_3)$

$$U_{e2} = \frac{\sin\theta}{\sqrt{1+\cos^2\theta}}\,, \quad U_{e3} = -\frac{1}{2}\frac{\sin 2\theta}{\sqrt{1+\cos^2\theta}}\,, \quad U_{\mu 3} = \frac{1}{\sqrt{2}}\frac{\sin^2\theta}{\sqrt{1+\cos^2\theta}}\,. \tag{6.1}$$

case (c2): $diag.(m_1, -m_2, m_3)$

$$U_{e2} = \sin\theta\,, \quad U_{e3} = \frac{1}{2}\frac{\sin 2\theta}{\sqrt{1+\sin^2\theta}}\,, \quad U_{\mu 3} = \frac{1}{\sqrt{2}}\frac{\cos^2\theta}{\sqrt{1+\sin^2\theta}}\,. \tag{6.2}$$

case (c3): $diag.(-m_1, -m_2, m_3)$

$$U_{e2} = 0\,, \quad U_{e3} = 0\,, \quad U_{\mu 3} = \frac{1}{\sqrt{2}}\,. \tag{6.3}$$

case (c4): $diag.(m_1, m_2, m_3)$

$$U_{e2} = 0\,, \quad U_{e3} = 0\,, \quad U_{\mu 3} = 0\,. \tag{6.4}$$

Results of this article are not only useful for the model building, but also show the possibility to obtain the large mixing angles from quantum corrections.

Acknowledgments

One of the author NO thanks G.-C. Cho and K. Hagiwara for useful discussion and comments. The work of NH is partially supported by DOE grant DOE/ER/01545-753. The work of NO is supported by the JSPS Research Fellowships for Young Scientists, No. 2996.

A Oscillation Probabilities in the Vacuum

The transition probability $P_{\nu_\alpha \to \nu_\beta}$, $(\alpha \neq \beta)$ and the survival probability $P_{\nu_\alpha \to \nu_\alpha}$ of the neutrino-oscillation are given by

$$\begin{aligned} P_{\nu_\alpha \to \nu_\beta} &= \left| \sum_{j=1}^{3} \left(V_{\rm MNS}\right)_{\beta j} \exp\left(\frac{-im_j^2}{2E}L\right) \left(V_{\rm MNS}^\dagger\right)_{j\alpha} \right|^2 , \\ &= \left| U_{\beta 1}U_{\alpha 1}^* + U_{\beta 2}\exp\left(\frac{-i\delta m_{12}^2}{2E}L\right)U_{\alpha 2}^* + U_{\beta 3}\exp\left(\frac{-i\delta m_{13}^2}{2E}L\right)U_{\alpha 3}^* \right|^2 , \quad \text{(A.1)} \end{aligned}$$

$$\begin{aligned} P_{\nu_\alpha \to \nu_\alpha} &= \left| \sum_{j=1}^{3} \left(V_{\rm MNS}\right)_{\alpha j} \exp\left(\frac{-im_j^2}{2E}L\right) \left(V_{\rm MNS}^\dagger\right)_{j\alpha} \right|^2 , \\ &= \left| U_{\alpha 1}U_{\alpha 1}^* + U_{\alpha 2}\exp\left(\frac{-i\delta m_{12}^2}{2E}L\right)U_{\alpha 2}^* + U_{\alpha 3}\exp\left(\frac{-i\delta m_{13}^2}{2E}L\right)U_{\alpha 3}^* \right|^2 , \quad \text{(A.2)} \end{aligned}$$

respectively. Here we note $\delta m_{ij}^2 = m_j^2 - m_i^2$. When $\delta m_{12}^2 \ll \delta m_{13}^2$, eqs.(A.1)and (A.2) can be simplified as follows.

Condition 1:

$$\frac{\delta m_{12}^2}{2E}L \ll 1 \sim \frac{\delta m_{13}^2}{2E}L \quad \text{(A.3)}$$

Under this condition, eq.(A.1) becomes

$$\begin{aligned} P_{\nu_\alpha \to \nu_\beta} &= \left| -U_{\beta 3}U_{\alpha 3}^* + U_{\beta 3}\exp\left(\frac{-i\delta m_{13}^2}{2E}L\right)U_{\alpha 3}^* \right|^2 , \\ &= 4\left|U_{\alpha 3}\right|^2 \left|U_{\beta 3}\right|^2 \sin^2\left(\frac{\delta m_{13}^2}{4E}L\right) , \quad \text{(A.4)} \end{aligned}$$

and eq.(A.2) becomes

$$\begin{aligned} P_{\nu_\alpha \to \nu_\alpha} &= \left| 1 - U_{\alpha 3}U_{\alpha 3}^* + U_{\alpha 3}\exp\left(\frac{-i\delta m_{13}^2}{2E}L\right)U_{\alpha 3}^* \right|^2 , \\ &= 1 - 4\left|U_{\alpha 3}\right|^2 \left(1 - \left|U_{\alpha 3}\right|^2\right) \sin^2\left(\frac{\delta m_{13}^2}{4E}L\right) . \quad \text{(A.5)} \end{aligned}$$

Condition 2:

$$\frac{\delta m_{12}^2}{2E}L \sim 1 \ll \frac{\delta m_{13}^2}{2E}L \quad \text{(A.6)}$$

Under this condition, eqs.(A.1) and (A.2) become

$$P_{\nu_\alpha\to\nu_\beta} = 2|U_{\alpha3}|^2|U_{\beta3}|^2 - \left[4Re(U_{\alpha1}U^*_{\beta1}U_{\beta2}U^*_{\alpha2})\sin^2\left(\frac{\delta m^2_{12}}{4E}L\right) + 2J_{\rm MNS}\sin\left(\frac{\delta m^2_{12}}{2E}L\right)\right], \tag{A.7}$$

$$P_{\nu_\alpha\to\nu_\alpha} = 1 - 2|U_{\alpha3}|^2\left(1-|U_{\alpha3}|^2\right) - 4|U_{\alpha1}|^2|U_{\alpha2}|^2\sin^2\left(\frac{\delta m^2_{12}}{4E}L\right), \tag{A.8}$$

respectively. Here $J_{\rm MNS}$ is defined by $Im(U_{\alpha1}U^*_{\beta1}U_{\beta2}U^*_{\alpha2})$.

B Quantum Corrections of κ

In this section, we show the relation between $\kappa(m_z)$ and $\kappa(M_R)$ in the cases of $\kappa_{33}=0$ and $\kappa_{11}=\kappa_{22}=\kappa_{33}=0$.

B.1 $\kappa_{33}=0$

At first, we discuss the case of $\kappa_{33}=0$ in the diagonal base of $y^{\rm e}$. If some elements of κ are zero at m_z, they are always zero through all energy-scale. This means if κ_{33} is zero at m_z, κ cannot be normalized by κ_{33} and c_{ij} of eq.(3.3) cannot be defined. Thus, we adopt κ_{22} for the normalization of κ as

$$\begin{aligned}\kappa &= \kappa_{22}\begin{pmatrix} r'_1 & c'_{12}\sqrt{r'_1} & c'_{13}r'_2\sqrt{r'_1} \\ c'_{12}\sqrt{r'_1} & 1 & r'_2 \\ c'_{13}r'_2\sqrt{r'_1} & r'_2 & 0 \end{pmatrix}, \\ &= \kappa_{22}\begin{pmatrix} \sqrt{r'_1} & 0 & 0 \\ 0 & 1 & 0 \\ 0 & 0 & r'_2 \end{pmatrix}\begin{pmatrix} 1 & c'_{12} & c'_{13} \\ c'_{12} & 1 & 1 \\ c'_{13} & 1 & 0 \end{pmatrix}\begin{pmatrix} \sqrt{r'_1} & 0 & 0 \\ 0 & 1 & 0 \\ 0 & 0 & r'_2 \end{pmatrix},\end{aligned} \tag{B.1}$$

where c'_{1j}s $(j=2,3)$ are defined as

$$(c'_{12})^2 = \frac{\kappa^2_{12}}{\kappa_{11}\kappa_{22}}, \quad \text{and} \quad (c'_{13})^2 = \frac{\kappa_{22}\kappa^2_{13}}{\kappa_{11}\kappa^2_{23}}, \tag{B.2}$$

which are energy-scale independent complex parameters. $r'_{1,2}$ in eq.(B.1) are defined as

$$r'_1 = \frac{\kappa_{11}}{\kappa_{22}}, \quad \text{and} \quad r'_2 = \frac{\kappa_{23}}{\kappa_{22}}. \tag{B.3}$$

By using the notation of eq.(3.8), we can obtain the energy-scale dependences of $r'_{1,2}$ as

$$r'_1(M_R) = r'_1(m_z)\frac{I_e}{I_\mu}\,, \quad \text{and} \quad r'_2(M_R) = r'_2(m_z)\sqrt{\frac{I_\tau}{I_\mu}}\,. \tag{B.4}$$

Then, $\kappa(M_R)$ is given by

$$\kappa(M_R) = \frac{k_{22}(M_R)}{k_{22}(m_z)}\frac{I_\tau}{I_\mu}\begin{pmatrix} \sqrt{I_e/I_\tau} & 0 & 0 \\ 0 & \sqrt{I_\mu/I_\tau} & 0 \\ 0 & 0 & 1 \end{pmatrix}\kappa(m_z)\begin{pmatrix} \sqrt{I_e/I_\tau} & 0 & 0 \\ 0 & \sqrt{I_\mu/I_\tau} & 0 \\ 0 & 0 & 1 \end{pmatrix}. \tag{B.5}$$

B.2 $\kappa_{11} = \kappa_{22} = \kappa_{33} = 0$

When all diagonal elements are zero, all off-diagonal elements of κ can be taken real. It is because all phases are absorbed by the field redefinitions of

$$L_i \to e^{-i\varphi_i}L_i\,, \quad \text{and} \quad E_i \to e^{i\varphi_i}E_i\,, \tag{B.6}$$

where φ_is are defined as

$$\begin{aligned} \varphi_1 &= \left(arg.(\kappa_{12}) + arg.(\kappa_{13}) - arg.(\kappa_{23})\right)/4\,, \\ \varphi_2 &= \left(arg.(\kappa_{12}) - arg.(\kappa_{13}) + arg.(\kappa_{23})\right)/4\,, \\ \varphi_3 &= \left(-arg.(\kappa_{12}) + arg.(\kappa_{13}) + arg.(\kappa_{23})\right)/4\,. \end{aligned} \tag{B.7}$$

Normalizing all elements by κ_{23}, κ is given by

$$\begin{aligned} \kappa &= \kappa_{23}\begin{pmatrix} 0 & r''_1 & r''_2 \\ r''_1 & 0 & 1 \\ r''_2 & 1 & 0 \end{pmatrix}, \\ &= \kappa_{23}\begin{pmatrix} \sqrt{r''_1 r''_2} & 0 & 0 \\ 0 & \sqrt{r''_1/r''_2} & 0 \\ 0 & 0 & \sqrt{r''_2/r''_1} \end{pmatrix}\begin{pmatrix} 0 & 1 & 1 \\ 1 & 0 & 1 \\ 1 & 1 & 0 \end{pmatrix}\begin{pmatrix} \sqrt{r''_1 r''_2} & 0 & 0 \\ 0 & \sqrt{r''_1/r''_2} & 0 \\ 0 & 0 & \sqrt{r''_2/r''_1} \end{pmatrix}, \end{aligned} \tag{B.8}$$

where

$$r''_1 = \frac{\kappa_{12}}{\kappa_{23}}\,, \quad \text{and} \quad r''_2 = \frac{\kappa_{13}}{\kappa_{23}}\,. \tag{B.9}$$

By using the notation of eq.(3.8), we can obtain $r''_{1,2}(M_R)$ as

$$r''_1(M_R) = r''_1(m_z)\sqrt{\frac{I_e}{I_\tau}}\,, \quad \text{and} \quad r''_2(M_R) = r''_2(m_z)\sqrt{\frac{I_e}{I_\mu}}\,. \tag{B.10}$$

Then, $\kappa(M_R)$ is given by

$$\kappa(M_R) = \frac{\kappa_{23}(M_R)}{\kappa_{23}(m_z)}\sqrt{\frac{I_\tau}{I_\mu}} \begin{pmatrix} \sqrt{I_e/I_\tau} & 0 & 0 \\ 0 & \sqrt{I_\mu/I_\tau} & 0 \\ 0 & 0 & 1 \end{pmatrix} \kappa(m_z) \begin{pmatrix} \sqrt{I_e/I_\tau} & 0 & 0 \\ 0 & \sqrt{I_\mu/I_\tau} & 0 \\ 0 & 0 & 1 \end{pmatrix} . \quad \text{(B.11)}$$

Equations (B.5) and (B.11) show that the energy-scale dependence of the MNS matrix can be estimated by $\sqrt{I_e/I_\tau}$ and $\sqrt{I_\mu/I_\tau}$ even in the cases of $\kappa_{33} = 0$ or $\kappa_{11} = \kappa_{22} = \kappa_{33} = 0$. In general, quantum corrections of the MNS matrix can be estimated by only $n_g - 1$ degrees of freedom. It is easily understood as follows. The RGE of κ (eq.(3.1)) is separated into two parts, which are the lepton-flavor independent terms (the gauge and the Higgs particles corrections) and the lepton-flavor dependent terms (the charged-lepton corrections). The energy-scale dependences of the mixing angles of κ are determined by the flavor-dependent corrections from $y^{\rm e}$. Since $y^{\rm e}$ has n_g degrees of freedom, expect for the over all factor, $n_g - 1$ degrees of freedom decide the energy-scale dependence of the MNS matrix as are shown in eqs.(3.9), (B.5) and (B.11).

C Approximation of the Renormalization Corrections

We show the approximation of $\sqrt{I_i/I_\tau}$. Although we do not use this approximation in our numerical analyses, it is useful for the rough estimation of quantum corrections of κ.

At first, let us estimate the values of

$$\frac{\sqrt{I_{e,\mu}/I_\tau} - \sqrt{1/I_\tau}}{\sqrt{I_{e,\mu}/I_\tau}} = 1 - \frac{1}{\sqrt{I_{e,\mu}}} . \quad \text{(C.1)}$$

The magnitudes of eq.(C.1) are estimated to be

$$0 < 1 - \frac{1}{\sqrt{I_e}} \ll 10^{-8} , \quad \text{and} \quad 0 < 1 - \frac{1}{\sqrt{I_\mu}} \ll 10^{-3} , \quad \text{(C.2)}$$

in the region of $2 \leq \tan\beta \leq 60$ from the numerical analysis shown in Figure 9. Thus, the approximation of

$$\sqrt{\frac{I_{e,\mu}}{I_\tau}} \simeq \frac{1}{\sqrt{I_\tau}} \quad \text{(C.3)}$$

is held with good accuracy. If we neglect the energy-scale dependence of y_τ, the value of

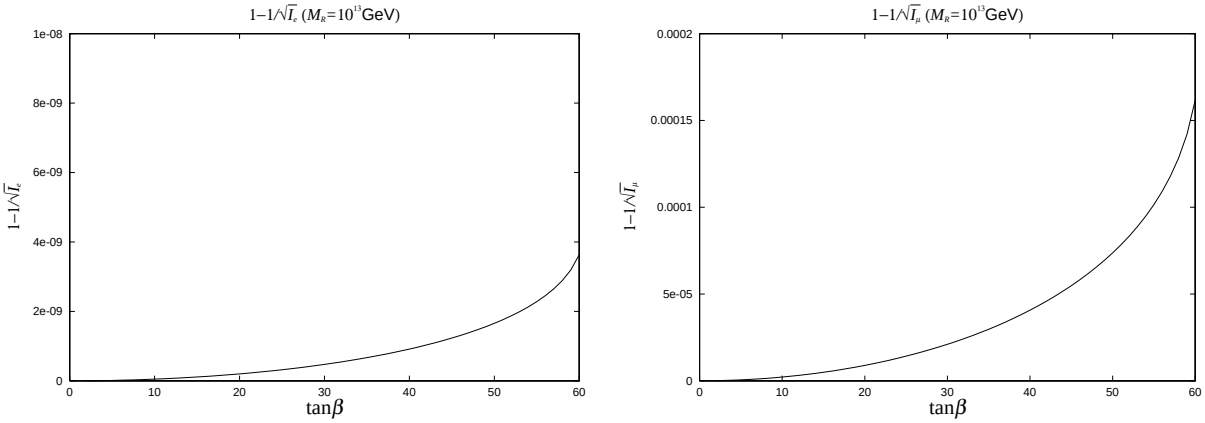

Figure 9: $\tan\beta$ dependences of eqs.(C.1).

eq.(C.3) is given by

$$\ln\left(\frac{1}{\sqrt{I_\tau}}\right) = \frac{1}{8\pi^2}\left(\frac{m_\tau}{v}\right)^2\left(\tan\beta^2+1\right)\ln\left(\frac{m_z}{M_R}\right) \tag{C.4}$$

from eq.(3.8), where m_τ is the mass of τ-lepton and $v^2 = \langle\phi_{\rm d}^2\rangle + \langle\phi_{\rm u}^2\rangle$. We define the faction of

$$Err(\tan\beta, M_R) = 1 - \sqrt{I_\tau} \times \left(\frac{m_z}{M_R}\right)^{\frac{1}{8\pi^2}\left(\frac{m_\tau}{v}\right)^2\left(\tan\beta^2+1\right)} \tag{C.5}$$

to check the accuracy of eq.(C.4). The $\tan\beta$ dependence of $|Err|$ is shown in Figure 10 with $M_R = 10^{13}$ GeV. In the region of $2 \leq \tan\beta \leq 50$, the error of eq.(C.4) is less than 1%. Even in the region of $50 \leq \tan\beta \leq 60$, where the energy scale dependence of y_τ cannot be neglected, $|Err|$ is less than 10%.

If M_R is smaller than 10^{13} GeV, the approximation of eq.(C.4) becomes more accurate because the Yukawa couplings of the charged-leptons are enhanced in the high energy scale.

References

[1] Homestake Collaboration, B.T. Cleveland *et al.*, Nucl. Phys.(Proc. Suppl.) **B38**, 47 (1995); Kamiokande Collaboration, Y. Suzuki, Nucl. Phys. (Proc. Suppl.) **B38**, 54 (1995); GALLEX Collaboration, P. Anselmann *et al.*, Phys. Lett. **B357**, 237 (1995); SAGE Collaboration, J.N. Abdurashitov *et al.*, Phys. Lett. **B328**, 234 (1994); Super-Kamiokande Collaboration, Phys. Pev. Lett. **82**, 1810 (1999); hep-ex/9812011; hep-ex/9903034.

[2] Kamiokande Collaboration, K.S. Hirata *et al.*, Phys. Lett. **B205**, 416 (1988); *ibid.* **B280**, 146 (1992); Y. Fukuda *et al.*, Phys. Lett. **B335**, 237 (1994); IMB Collaboration,

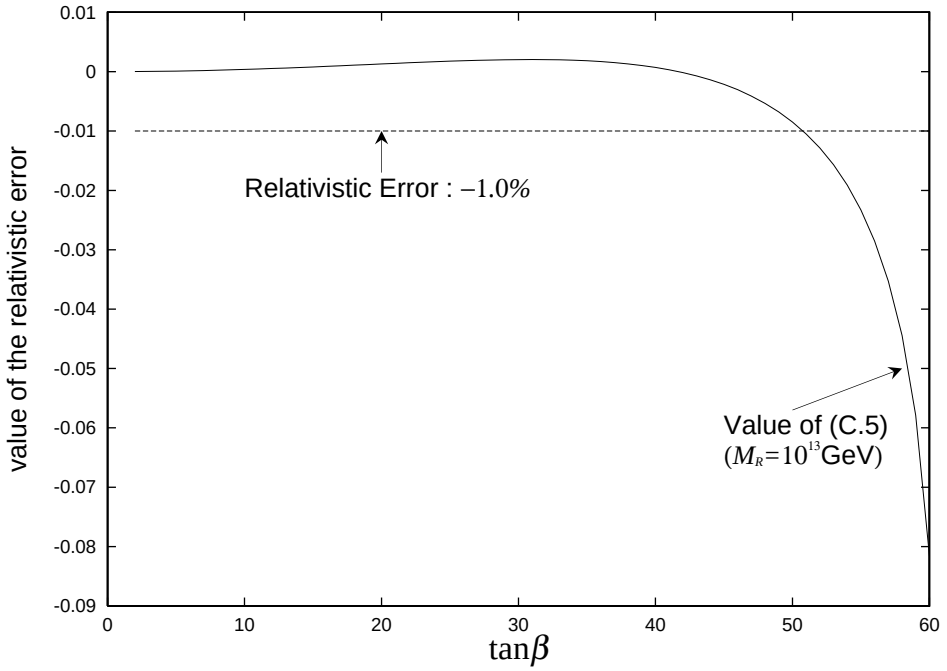

Figure 10: $\tan\beta$ dependence of eq.(C.5).

D. Casper *et al.*, Phys. Pev. Lett. **66**, 2561 (1991); R. Becker-Szendy *et al.*, Phys. Rev. **D46**, 3720 (1992); SOUDAN2 Collaboration, T. Kafka, Nucl. Phys. (Proc. Suppl.) **B35**, 427 (1994); M.C. Goodman, *ibid.* **38**, (1995) 337; W.W.M. Allison *et al.*, Phys. Lett. **B391**, 491 (1997); hep-ex/9901024 to be published in Phys. Lett. B.

[3] Y. Totsuka, invited talk at the 18th International Symposium on Lepton-Photon Interaction, July 28 - August 1, 1997 Hamburg; Super-Kamiokande Collaboration, Phys. Pev. Lett. **81**, 1562 (1998); Phys. Pev. Lett. **82**, 2644 (1999); hep-ex/9903047.

[4] The CHOOZ Collaboration, Phys. Lett. **B420**, 397 (1998).

[5] Z.Maki, M.Nakagawa and S.Sakata, Prog. Theor. Phys. **28**, 870 (1962).

[6] *See, for example,*
M. Bando, Izawa Ken-Iti and T. Takahashi, Prog. Theor. Phys. **92**, 1137 (1994); M. Schmaltz, Phys. Rev. **D52**, 1643 (1995); Y. Achiman and T. Greiner, Nucl. Phys. **B443**, 3 (1995); G.K. Leontaris, S. Lola and G.G. Ross, Nucl. Phys. **B454**, 25 (1995); M. Tanimoto, Phys. Lett. **B360**, 41 (1995); G.K. Leontaris and S. Lola, hep-ph/9510340; Mar Bastero-Gil and B. Brahmachari, Nucl. Phys. **B482**, 39 (1996); G. Lazarides, Q. Shafi and N.D. Vlachos, Phys. Lett. **B427**, 53 (1998); M.K. Parida and N. Nimai Singh, Phys. Rev. **D59**, 032002 (1999); B. Brahmachari and R.N. Mohapatra, Phys. Rev. **D58**, 015003 (1998); N. Haba and T. Matsuoka, Prog. Theor. Phys. **99**, 831 (1998); G. Lazarides, hep-ph/9801340; C.H. Albright, K.S. Babu and S.M. Barr, Phys. Pev. Lett. **81**, 1167 (1998); G. Lazarides, hep-ph/9802415; B.C. Al-

lanach, Phys. Lett. **B450**, 182 (1999); M. Tanimoto, hep-ph/9807517; N. Haba, Phys. Rev. **D59**, 035011 (1999); J. Ellis, G.K. Leontaris, S. Lola and D.V. Nanopoulos, hep-ph/9808251; S. Lola, G.G. Ross, hep-ph/9902283; Y. Nir and Y. Shadmi, JHEP 9905 023 (1999); S. Lola, hep-ph/9903203; J.A. Casas, J.R. Espinosa, A. Ibarra and I. Navarro, hep-ph/9904395; J.A. Casas, J.R. Espinosa, A. Ibarra and I. Navarro, hep-ph/9905381; J.A. Casas, J.R. Espinosa, A. Ibarra and I. Navarro, hep-ph/9906281; M. Carena, J. Ellis, S. Lola and C.E.M. Wagner, hep-ph/9906362; R. Barbieri, G.G. Ross and A. Strumia, hep-ph/9906470.

[7] G. Altarelli and F. Feruglio, hep-ph/9809596.

[8] N. Cabibbo, Phys. Pev. Lett. **10**, 531 (1964); M. Kobayashi and T. Maskawa Prog. Theor. Phys. **49**, 652 (1973).

[9] Particle Data Group. The European Physical Journal **C3**, 1 (1998); htt://pdg.lbl.gov.

[10] L. Wolfenstein. Phys. Pev. Lett. **51**, 1945 (1983).

[11] M. Kobayashi, Prog. Theor. Phys. **92**, 287 (1994); *ibid* **92**, 289 (1994).

[12] K. Hagiwara and N. Okamura, Nucl. Phys. **B548**, 60 (1999).

[13] L. Wolfenstein, Phys. Rev. **D17**, 2369 (1978); S.P. Mikheyev and A.Yu. Smirnov, Yad. Fiz. **42**, 1441 (1985) [Sov.J.Nucl.Phys.**42**, 913 (1986)]; Nuovo Cimento **C9**, 17 (1986).

[14] B. Pontecorvo, Zh.Eksp. Teor. Fiz. **53**, 1717 (1967); S.M. Bilenky and B. Pontecorvo, Phys. Rep. **41**, 225 (1978); V. Barger, R.J.N. Phillips and K. Whisnant, Phys. Rev. **D24**, 538 (1981); S.L. Glashow and L.M. Krauss, Phys. Lett. **190B**, 199 (1987).

[15] P.H. Chankowski and Z. Pluciennik, Phys. Lett. **316B**, 312 (1993).

[16] K.S. Babu, C.N. Leung and J. Pantaleone, Phys. Lett. **319B**, 191 (1993).

[17] T. Yanagida, in *Proceedings of the Workshop on Unified Theory and Baryon Number in the Universe*, ed. O. Sawada and A. Sugamoto (KEK, report 79-18, 1979), p.95;
M. Gell-Mann, P. Ramond and S. Slansky, in *Supergravity*, ed. P. van Nieuwenhuizen and D.Z. Freedman (North-Holland, Amsterdam, 1979), p315;
R. Mohapatra and S. Senjanović, Phys. Pev. Lett. **44**, 912 (1980).

[18] N. Haba, Y. Matsui, N. Okamura and M. Sugiura, hep-ph/9904292, to be published in Euro. Phys. Jour. C.

[19] N. Haba, N. Okamura and M. Sugiura, hep-ph/9810471.

[20] H. Georgi and S.L. Glashow, hep-ph/9808293.

[21] L. Baudis and *et al.*, hep-ex/9902014.

[22] J. Ellis and S. Lola, hep-ph/9904279.